AD-A174 970 PLASMA DEPOSITION OF SILICON CARBIDE THIN FILMS(U) 1/1
WESTINGHOUSE RESEARCH AND DEVELOPMENT CENTER PITTSBURGH
PA W D PARTLOW ET AL. 30 JUL 86 AFOSR-TR-86-2038
UNCLASSIFIED F49620-84-0063 F/G 7/4 NL

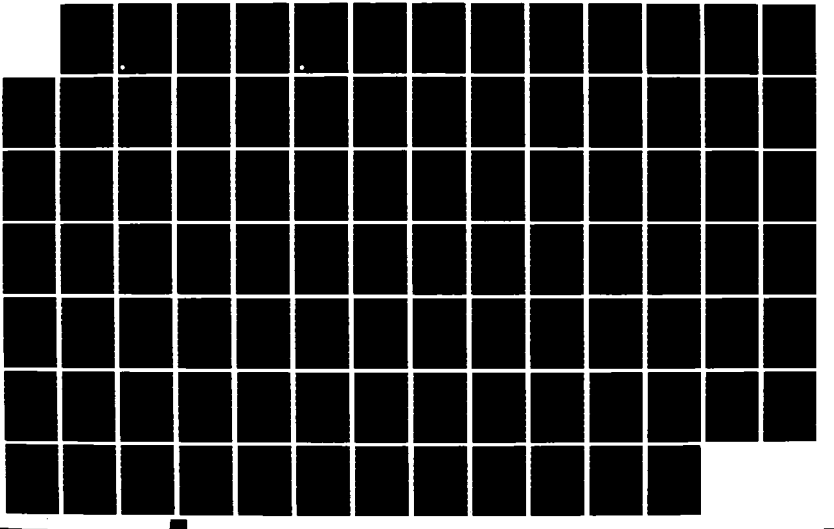

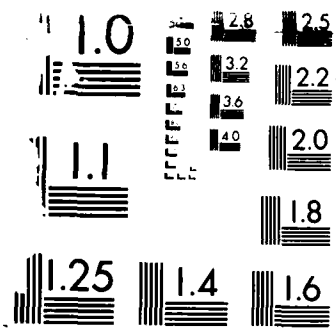
1.0
1.1
1.25
1.4
1.6
1.8
2.0
2.2
2.5
2.8
3.2
3.6
4.0
RESOLUTION TEST CHART

AFOSR-TR- 86-2038

(2)

PLASMA DEPOSITION OF SILICON CARBIDE THIN FILMS

W. D. Partlow, W. J. Choyke, John T. Yates, Jr.,
L. E. Kline, M. J. Bozack, L. Muehloff,
P. A. Taylor, A. Mascarenhas, J.V.R. Heberlein

Annual Technical Report No. 2
Report Period Covered
July 1, 1984 to June 30, 1986

Contract No. F49620-84-C-0063DEF

July 30, 1986

Air Force Office of Scientific Research
Bolling Air Force Base
Washington, DC 20332

Captain Kevin J. Malloy
Program Manager

Westinghouse R&D Center
General Order Number WGD-11481-CE

Westinghouse R&D Center
1310 Beulah Road
Pittsburgh, Pennsylvania 15235

SECURITY CLASSIFICATION OF THIS PAGE (When Data Entered)

REPORT DOCUMENTATION PAGE		READ INSTRUCTIONS BEFORE COMPLETING FORM
1. REPORT NUMBER AFOSR-TR- 86-2038	2. GOVT ACCESSION NO. ADA174920	3. RECIPIENT'S CATALOG NUMBER
4. TITLE (and Subtitle) PLASMA DEPOSITION OF SILICON CARBIDE THIN FILMS		5. TYPE OF REPORT & PERIOD COVERED Annual 7-1-84 to 6-30-86
		6. PERFORMING ORG. REPORT NUMBER
7. AUTHOR(s) W. D. Partlow, W. J. Choyke, John T. Yates, Jr., L. E. Kline, M. J. Bozack, L. Muelhoff, P. A. Taylor, A. Mascarenhas, J.V.R. Heberlein		8. CONTRACT OR GRANT NUMBER(s) F49620-84-C-0063DEF
9. PERFORMING ORGANIZATION NAME AND ADDRESS Westinghouse R&D Center, 1310 Beulah Road, Pittsburgh, PA 15235		10. PROGRAM ELEMENT, PROJECT, TASK AREA & WORK UNIT NUMBERS 61102F 2305/B1
11. CONTROLLING OFFICE NAME AND ADDRESS Air Force Office of Scientific Research Boling Air Force Base Washington, DC 20332 NE		12. REPORT DATE July 30, 1986
		13. NUMBER OF PAGES 87
14. MONITORING AGENCY NAME & ADDRESS(if different from Controlling Office) Same as 11		15. SECURITY CLASS. (of this report) UC
		15a. DECLASSIFICATION/DOWNGRADING SCHEDULE

16. DISTRIBUTION STATEMENT (of this Report)

Approved for public release; distribution unlimited.

17. DISTRIBUTION STATEMENT (of the abstract entered in Block 20, if different from Report)

Approved for public release; distribution unlimited.

18. SUPPLEMENTARY NOTES

19. KEY WORDS (Continue on reverse side if necessary and identify by block number)

Plasmas, Deposition, Thin Films Silicon Carbide, Surfaces, Desorption, UHV.

20. ABSTRACT (Continue on reverse side if necessary and identify by block number)

In this reporting period, the second year of a three-year program, the two major thrusts of the program produced significant achievements along independent lines, having spent the first year of the program preparing and testing the equipment and beginning the experiments. Mid-program planning and discussion sessions have led to the planning of two experimental studies that will tie together the work of the two groups. The first of three experiments has been completed.

(over)

DD FORM 1 JAN 73 1473 EDITION OF 1 NOV 65 IS OBSOLETE

SECURITY CLASSIFICATION OF THIS PAGE (When Data Entered)

In the plasma studies area, the model for carbon deposition from methane plasmas was extended to include homogeneous chemical kinetics of both neutral and ionized species, and it was tested with extensive plasma characterization experiments varying plasma excitation and flow parameters. In addition, experiments were completed on methane-hydrogen plasmas, and we plan to compare these results to the model.

Thermal desorption and dissociation kinetic studies of propylene on silicon surfaces has produced several significant results. It was found that surface reactivity could be controlled by creating damage sites via ion bombardment or by capping such sites with atomic hydrogen. In addition, the adsorption of propane and methane were studied AT 120K and compared to the double-bonded propylene using kinetic uptake experiments and Auger surface studies. It was found that no sticking is obtained for hydrocarbon molecules that do not have C=C double bonds.

This program has produced several journal articles as well as numerous invited and contributed conference talks and papers. Four preprints are attached which describe the main accomplishments of this program during this reporting period.

PLASMA DEPOSITION OF SILICON CARBIDE THIN FILMS

W. D. Partlow, W. J. Choyke, John T. Yates, Jr.,
L. E. Kline, M. J. Bozack, L. Muehloff,
P. A. Taylor, A. Mascarenhas, J.V.R. Heberlein

Annual Technical Report No. 2
Report Period Covered
July 1, 1984 to June 30, 1986

Contract No. F49620-84-C-0063DEF

July 30, 1986

Air Force Office of Scientific Research
Bolling Air Force Base
Washington, DC 20332

Captain Kevin J. Malloy
Program Manager

Westinghouse R&D Center
General Order Number WGD-11481-CE

Westinghouse R&D Center
1310 Beulah Road
Pittsburgh, Pennsylvania 15235

ANNUAL REPORT: PLASMA DEPOSITION OF SILICON CARBIDE FILMS

JULY 30, 1986

ABSTRACT

In this reporting period, the second year of a three-year program, the two major thrusts of the program produced significant achievements along independent lines, having spent the first year of the program preparing and testing the equipment and beginning the experiments. Mid-program planning and discussion sessions have led to the planning of two experimental studies that will tie together the work of the two groups. The first of these experiments has been completed.

In the plasma studies area, the model for carbon deposition from methane plasmas was extended to include homogeneous chemical kinetics of both neutral and ionized species, and it was tested with extensive plasma characterization experiments varying plasma excitation and flow parameters. In addition, experiments were completed on methane-hydrogen plasmas, and we plan to compare these results to the model.

Thermal desorption and dissociation kinetic studies of propylene on silicon surfaces has produced several significant results. It was found that surface reactivity could be controlled by creating damage sites via ion bombardment or by capping such sites with atomic hydrogen. In addition, the adsorption of propane and methane were studied at 120K and compared to the double-bonded propylene using kinetic uptake experiments and Auger surface studies. It was found that no sticking is obtained for hydrocarbon molecules that do not have C=C double bonds.

This program has produced several journal articles as well as numerous invited and contributed conference talks and papers. Four preprints are attached which describe the main accomplishments of this program during this reporting period.

I OVERVIEW

Having prepared the equipment and carried out preliminary experiments needed to characterize the experimental apparatus in the first year of the program, our objectives were to focus on experiments that would provide information on the fundamental plasma deposition processes. We had begun studying the deposition of carbon with pure hydrocarbon gases, and we continued this approach. Rather than adding silane chemistry to produce silicon carbide, we found that concentrating on the simpler problem of carbon deposition provided an opportunity for a deeper understanding of the processes, and avoids duplication of significant work that is being done elsewhere on silane plasma chemistry, for example, by Alan Garscadden and his group at Wright -Patterson AFB in Dayton, Ohio. In the following sections we describe the contributions of the two groups:

a) plasma characterization and modeling at Westinghouse R&D Center;

b) surface studies at the Univ. of Pittsburgh Surface Science Center.

These two components of the program had proceeded relatively independently until the first experiments had been completed and analyzed at about mid-program in January, 1986. At this juncture we got together, made presentations of the results of the different groups, and discussed how they related to our overall objectives.

Two proposals came out of these discussions for experiments which would tie the two efforts together, allowing each group to capitalize on the progress of the other. The plasma group had found that quantitative surface adsorption data are needed for the methane deposition model, so experiments on the adsorption of methane and propane on silicon surfaces were planned. This would compare the adsorption of hydrocarbon gases without C=C double bonds to the extensive results that the group had already obtained on propylene, which has one C=C double bond. An additional

set of experiments was proposed to compare plasma deposition results using propylene gas to existing data for methane. Deposition processes uniquely associated with the C=C double bond in propylene had been identified by the surface chemistry group. These may lead to higher deposition rates or other advantages, so it is of interest to see if significant effects can be identified in plasma experiments. At this time, the first of these two experiments has been completed. Earlier expectations of the role of the C=C double bond in Si(100) adsorption have been substantiated, and guidance in modeling adsorption reactions from the plasma has been provided.

II PLASMA STUDIES

The characterization and modeling study of methane deposition plasmas was expanded in this period. The model produced in a collaborative effort by L. E. Kline on a Westinghouse-funded program was extended to include the homogeneous kinetic chemistry of both neutral and ionized dissociation products. This put us in a position to obtain information about the surface deposition kinetics by postulating likely surface reactions, including them in the model, and comparing the predictions of the model to our experimental results. The plasma experiments included mass spectroscopy and sample weighing to determine mass transfer in the plasmas, and also electrical waveform and probe measurements on the plasmas. In this way we have identified deposition reactions that lead to a consistent picture of the deposition chemistry. These results are reported in detail in Reference 1, which is attached. We have taken data over a wider range of experimental conditions since this was published, particularly, for a variety of gas flow rates and also for methane-hydrogen mixtures. This will test the model over a broader range of parameters and will also provide information about the role of hydrogen in deposition plasmas. Hydrogen has long been known to have a significant influence on the deposited films, in passivation dangling bonds for example, in amorphous silicon. More subtle involvement of hydrogen in the deposition processes has been suggested, both in low and high temperature processes. It is considered crucial for the production of CVD diamond films at higher temperatures. Our existing model already includes hydrogen, since it is one of the main products in the electron dissociation of methane. We have performed plasma deposition and characterization experiments with methane-hydrogen plasmas, and plan to compare the data to the model. Early experimental results point out an interesting interplay between flow rates and methane/hydrogen ratio. Significant enhancement of hydrogen mole fractions is obtained at low flow rates because of methane dissociation.

III CHARACTERIZATION

We have a set of samples of carbon films for a wide range of deposition conditions. This includes high and low energy ion bombardment conditions for samples prepared on the powered electrode and the grounded electrode respectively. Samples were prepared with a variety of power densities and flow rates. Recently we prepared a series of samples from methane-hydrogen mixtures. The goals of the characterization measurements are to understand the influence of these deposition conditions on the properties of the films, and to relate them to the plasma properties, which are fairly well characterized now. We will begin with reflectivity measurements to determine the optical gap of the films, and will study the carbon bonds via infrared and Raman spectra.

IV SURFACE STUDIES

A comprehensive study of the adsorption kinetics of propylene on Si(100) surfaces was performed during this reporting period using molecular beam techniques, thermal desorption techniques and Auger surface analysis. Two different types of adsorption processes were identified: one that results in dissociation of the propylene, and one in which undissociated propylene chemically bonds to the surface, and will desorb intact at 550K. On thermally annealed and ordered Si(100) surfaces, only about 65% of the propylene adsorption is dissociative. This fraction can be increased to nearly 100% by producing additional active sites via ion pre-bombardment of the surface, and the reactivity can be suppressed by capping the active sites with atomic hydrogen. This work is described in detail in Reference 2 and in Reference 3 which fully describes the techniques and apparatus. Preprints of these articles are attached.

As we mentioned in Section I, experiments to compare the adsorption of

propylene to hydrocarbons without C=C double bonds were recently completed. They are discussed in detail in Reference 4 which is attached. No adsorption could be measured for annealed or for ion-bombarded surfaces for methane or propane at 120K. This is convincing evidence of the role of the C=C double bond in the adsorption mechanism, and it also tells us that this type of ion-assisted deposition process is probably not nearly as important in methane deposition plasmas as it would be in propylene plasmas. This is consistent with our experimental and modeling conclusions, which attribute carbon deposition to neutral and ionized radicals rather than adsorbed reactant species. The importance of this latter type of deposition process in propylene plasmas, however, will be experimentally determined.

REFERENCES

1. W. D. Partlow and L. E. Kline, "Homogeneous and Heterogeneous Chemistry of Methane Deposition Plasmas", Proceedings of the 1986 Spring Meeting of the Materials Research Society, Symposium C: Plasma Processing, April, 1986.

2. M. J. Bozack, W. J. Choyke, L. Muehlhoff, and J. T. Yates, Jr., "Reaction Chemistry at the Si(100) Surface- Control Through Active Site Manipulation", accepted for publication, J. Appl. Phys.

3. M. J. Bozack, L., Muehlhoff, J. N. Russell, Jr., W. J. Choyke, and J. T. Yates, Jr., "Methods in Semiconductor Surface Chemistry" accepted for publication, J. Vac. Sci. Tech.

4. M. J. Bozack, P. A. Taylor, W. J. Choyke, and J. T. Yates, Jr., "Chemical Activity of the C=C Double Bond on Silicon Surface", accepted for publication, Surface Science.

APPENDIX

REFERENCE 1

HOMOGENEOUS AND HETEROGENEOUS CHEMISTRY OF METHANE DEPOSITION PLASMAS*

W. D. Partlow and L. E. Kline
Westinghouse R&D Center, 1310 Beulah Road, Pittsburgh, PA 15235

Experimental measurements and theoretical modeling of methane deposition plasmas have made it possible to determine the most likely homogeneous and heterogeneous chemical reaction paths leading to deposition of hydrogenated carbon from the fragments of electron dissociated methane. The methane plasma was modeled as a plug-flow reactor. Gas phase reactions, diffusive transport, variable surface reflection coefficients, and surface chemical reactions are included in the model which follows a "plug" of gas as it flows through the reactor. Boltzmann equation and Monte Carlo calculations were used to determine the electron energy distribution and the resulting dissociation and ionization rate coefficients averaged over space and time. Experimental measurements of the time dependent electrical properties of the plasma are used as input to the model. Deposition rates, deposition uniformity, downstream mass spectroscopy, and the dependences of these quantities on power and mass flow rates are compared to the model to arrive at a consistent representation of the deposition chemistry.

INTRODUCTION

The chemistry involved in the deposition of condensed phases from glow discharge plasmas consists of a highly complicated chain of processes starting with the electron dissociation of the reactant gases and concluding with heterogeneous surface deposition reactions, with homogeneous gas phase reactions in between. The deposition of hydrogenated carbon films from methane plasmas is an excellent example for study. Data is available on dissociation cross sections and fragmentation for this gas [1,2], and since methane is a widely used combustion gas, gas phase chemistry has been studied extensively. The chemical kinetics data for this gas has recently been pulled together by NBS workers and issued as a compendium [3]. Ion-neutral chemical kinetics data are also available [4]. A steady state model of the gas phase chemistry of methane plasmas has recently been published [5]. Our work carries this approach several steps further, in that it takes gas flow rates into account, providing spatial dependences not obtained in the earlier model. Also, more recent and complete gas phase reaction data is used in the model, and our more extensive experimental measurements, especially mass transport data, made it possible for us to study the heterogeneous chemistry in more detail.

Our work consists of an interactive experimental-theoretical study of these plasmas in which we have:

1) characterized the plasmas to define the parameters needed to perform the modeling,

2) modeled the dissociation and homogeneous chemistry using published gas physical and chemical data,

*This work was supported in part by the U. S. Air Force Office Of Scientific Research under contract F49260-84-C-0063DEF.

3) performed the model calculations with likely gas surface reactions, obtaining predictions of mass transport in the plasma,

4) compared the models containing these heterogeneous reactions to experimental mass transport data in the plasma to determine which of the reactions are most consistent with the experiments.

This has determined the most likely reaction paths for the deposition chemistry and has pointed out some additional experiments and calculations that can lead to more conclusive information about the plasma-surface deposition reactions.

EXPERIMENTS

Apparatus

The experimental deposition reactor is shown schematically in Figure 1. It consists of a pyrex pipe vacuum system with 8.9 cm planar electrodes. The powered lower electrode shown is a tri-axial design which can achieve self bias voltages of more than 1 kV, and the upper electrode shown has a floating probe diagnostic. Another electrode which can hold a substrate is used as the upper electrode during deposition, so that samples can be deposited on both the powered and the grounded electrodes in the same experiment. Gas flow and pressure are measured and controlled with electronic flow controllers and a capacitance manometer. A diffusion pumped system with a liquid nitrogen cold trap is used to obtain a base pressure below (10)-5 torr, and a 100CFM roots blower is used for high volume pumping during deposition. Downstream mass spectra are measured with a Dycor MI00 quadrupole gas analyzer in conjunction with a UTI turbo-pumped sampling system having a base pressure of (10)-9 torr. A Tektronix Model 7834 oscilloscope with a Model AM503 current probe were used to measure voltage and current waveforms. These waveforms were digitized to determine the electrical power delivered to the plasma. Average values of electrode bias

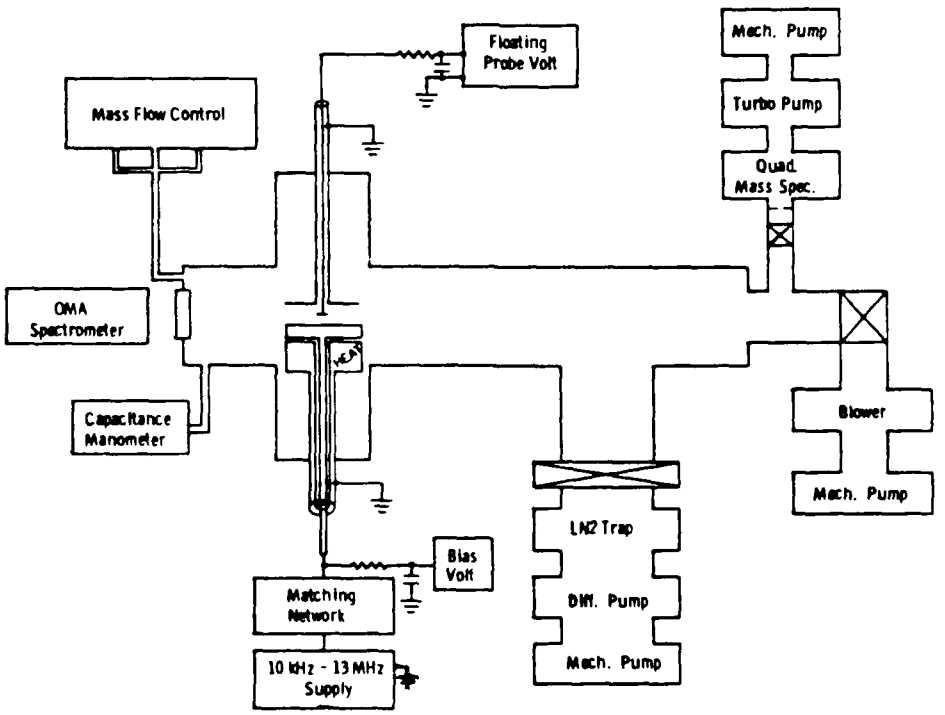

Figure 1. Schematic diagram of the experimental plasma deposition apparatus.

and floating probe potential were monitored with Keithley Model 600A electrometers with RC averaging circuits as shown schematically in Figure 1. Series resistor values of 10 MΩ were found to sufficiently large that no interaction of the measuring circuit with the experiment was seen. Capacitance values of 100pfd were adequate for averaging. The plasmas were powered with 2MHz RF excitation that was provided by an ENI Model 2100L RF power amplifier, using a Heath Model SA 2060A antenna tuner as a matching network.

Experimental Results

The electrical measurements on the plasma are summarized in Figure 2 for a methane plasma, 300 mtorr pressure, with flow rate of 30sccm. Peak-to-peak applied voltages from 700V to 1300V are measured for powers from 2 to 20 watts delivered to the plasma. Bias values for the powered electrode are shown for this range of powers, and are typically 30% of the peak-to peak voltage for these pressures and frequencies. Floating probe potential measured with the high impedance averaging circuit on a 1 cm diameter disc in the center of the plasma ranged from 0 to 19V. Based of the argument presented by Chapman [6], the average plasma potential is expected to be 10 to 15 volts above the floating probe potential, so we have established a condition where the sheath voltage is much higher at the powered electrode (several hundred volts) as compared to the sheath voltage at the grounded electrode (tens of volts).

We studied the mass transport in the reactor two ways: measuring the partial pressures of reactant and product gases downstream with a quadrupole mass spectrometer, and measuring the masses of the deposited films by weighing the silicon wafer substrates on a microbalance before and after deposition. The results of the weight-gain measurements are shown in Figure 3. The weight gain is attributed entirely to carbon since the mass of hydrogen is only 8% of that of carbon, and hydrogen has been found to be a minority constituent of plasma deposited carbon films [7]. The data show

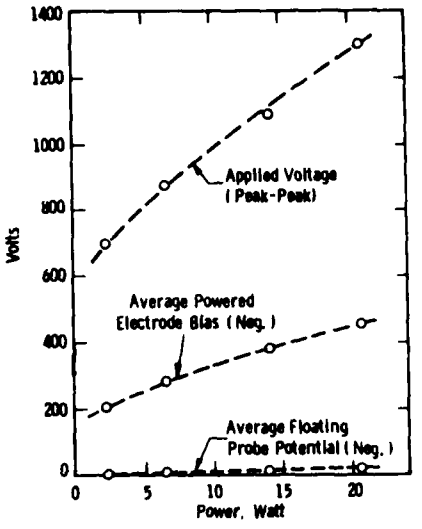

Figure 2. Peak-to-peak applied voltage, average electrode bias voltage, and average floating probe potential versus RF power of a methane plasma at 3000 mtorr pressure, 30 sccm flow rate, 2 MHz excitation frequency.

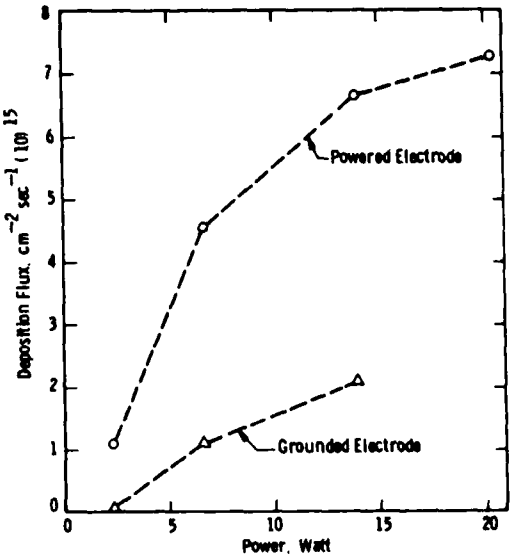

Figure 3. Carbon deposition flux versus power on substrates located on the two electrodes, 300 mtorr pressure, 30 sccm flow rate, 2MHz excitation frequency.

an increase in deposition flux with plasma power, and also that the deposition flux is several times higher on the powered electrode than on the grounded electrode, indicating that the higher negative bias voltages lead to higher deposition rates.

The mass spectroscopy cracking patterns measured downstream for three values of RF excitation power are shown in Figure 4. Ignoring masses 28 and 44 which are dominated by impurities in the quadrupole detector head, we can measure the mass peaks over a dynamic range of four decades. At zero power (no plasma) we see the cracking pattern for 99.99% pure research grade methane, which contains several lines between masses 25 and 30 along with the expected CH_4 lines between 12 and 18, indicating that there is some reaction in the mass spectrometer of species produced by the dissociation of methane or the purity of our methane may be as low as 99.9%. The following two traces taken at higher powers show increases in signals at high mass numbers, resulting from chemical reactions of the fragments produced by the electron dissociation of methane in the plasma. Based on calibrations of our mass spectrometer with pure gases of CH_4, C_2H_4, C_2H_6, C_3H_8, and C_4H_{10}, we selected mass numbers for each of the higher hydrocarbon groups, C_2H_X, C_3H_X, etc., which did not significantly overlap the cracking patterns of other species. This is possible in our experiments because the higher hydrocarbons are always less abundant than the lower ones, so the interferences from the low mass signals from these higher mass species are small. The hydrocarbon groups can be resolved into the component species only in the simplest case, C_2H_X, which was found to consist of about 70% C_2H_6, 30% C_2H_4, and a few percent of a lower mass component (probably C_2H_2). A plot of the mass signals from the different hydrocarbon groups, and H_2, is shown versus excitation power in Figure 5. It shows the CH_4 signal decreasing with power as H_2 and the higher hydrocarbons increase.

Based on the weight gain measurements and estimates of product gas pressures via mass spectroscopy, we have accounted for the total mass transport in the reactor to compare to the theoretical calculations. This is illustrated for one set of conditions in Figure 6, showing that the net

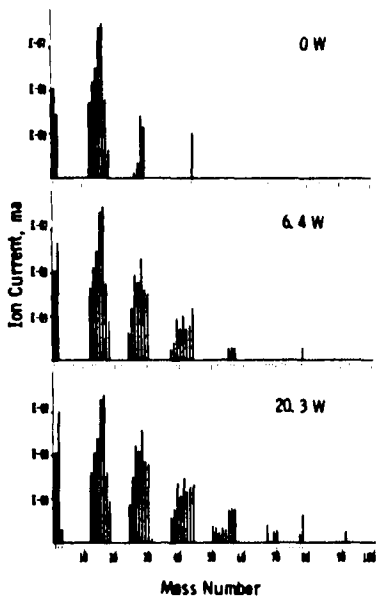

Figure 4. Cracking patterns in the mass spectra sampled downstream from a methane plasma at 300 mtorr pressure, 30 sccm flow rate, 2 MHz excitation frequency.

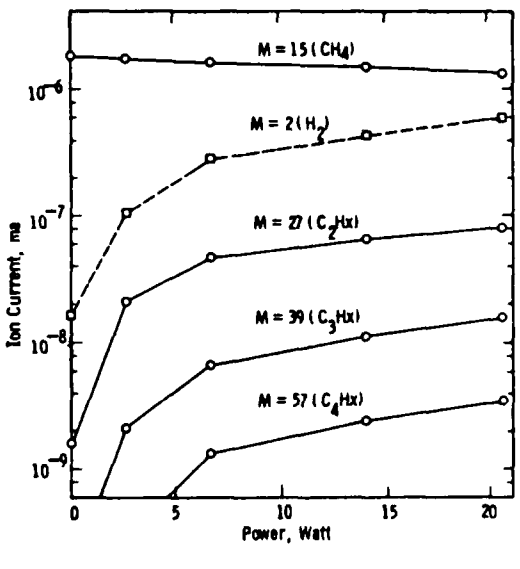

Figure 5. Ion currents of the species in the exhaust gases, versus RF excitation, of a methane plasma at 300 mtorr pressure, 30 sccm flow rate, 2 MHz excitation frequency.

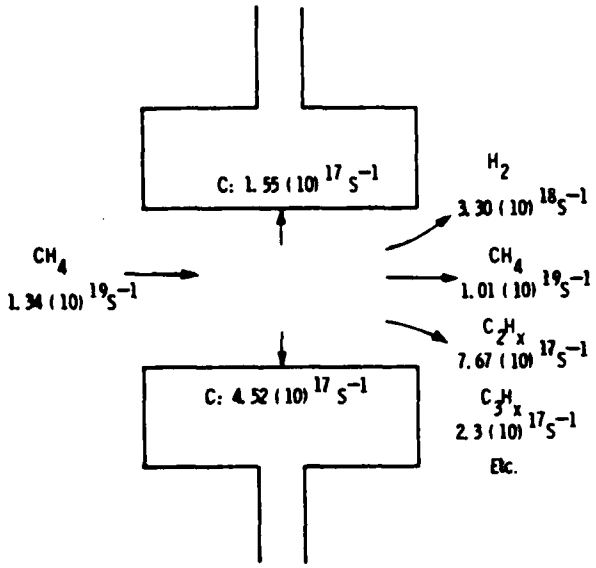

Figure 6. Mass transport of carbon in the reactor at 20 W power, 300 mtorr pressure, 30 sccm flow rate, 2 MHz excitation frequency.

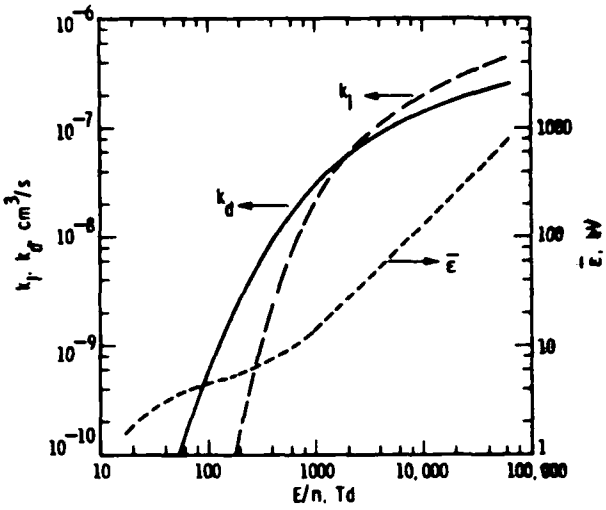

Figure 7. Average electron energy and the rate coefficients for dissociation and ionization versus E/n for methane.

dissociation of methane is about 25%, and that 5% of the carbon entering the reactor is deposited on the electrodes and 17% is found in the higher hydrocarbon exhaust gases up to C_3H_x, balancing the net carbon flux within experimental error. We can not measure the hydrogen mass balance.

ELECTRON KINETICS CALCULATIONS

The E/n values in typical RF deposition discharges are in the range 1000 to 100,000 Td where one Td (Townsend) = 1 x 10^{-17} volt cm^2. E/n is the electric field to gas density ratio. E/n is the scaling parameter for the electron energy distribution and the rate coefficients for electron impact dissociation and ionization. Furthermore, these E/n values are average fields given by:

$$(E/n)_{avg} = V_{avg}/nd$$

where V_{avg} is the average magnitude of the applied RF voltage, n is the gas density, and d is the electrode separation. The local field near the instantaneous cathode is even higher as shown by the experimental observations of Gottscho and Mandich [8] where the peak field is about 6 times as high as the average field at the time of the peak applied voltage.

The discharge electrons gain energy from the applied electric field and lose energy primarily in electron-neutral collisions in the weakly ionized conditions which are typical of low pressure RF plasma etching discharges. Two methods have been used to study the electron kinetics:

1) A relaxation method which finds the steady state electron energy distribution by solving a time dependent version the the electron Boltzmann equation and

2) A Monte Carlo simulation method which simultaneously follows a large number of electron trajectories in space and time.

The Boltzmann calculations use the formulation described by Rockwood [9] and a computer code developed by Lacina [10]. The electron energy distribution is represented by a two term spherical harmonic expansion in velocity space. The loss of electron in attachment as well as the production of secondary electron in ionization are taken into account. The secondary electrons are added at zero energy. A time dependent version of the Boltzmann equation is solved numerically in order to find the steady state distribution function. The formulation of the Monte Carlo model is described in Ref. 11. Its assumptions are identical to those of the Boltzmann equation model. Both vibrational excitation and dissociation are included in the calculations. These two processes have non zero cross sections in disjoint energy ranges with the CH_4 cross section set used here.

Electron Kinetics Results

The results of steady state electron energy distributions obtained by numerically solving the Boltzmann equation are shown in Figure 7. The quantities plotted include the average electron energy, $\bar{\varepsilon}$, and the rate coefficients for dissociation and ionization, k_d and k_i. An estimate of the time scale for relaxation of the electron energy distribution is given by:

$$t = \bar{\varepsilon}/EW \sim (D/\mu)/EW$$

where D is the electron diffusion coefficient and $\mu = W/E$ is the electron mobility. When the calculated mean energy is used in this expression t can be obtained from the results of the steady state electron energy distribution calculations. If D/μ is used as a measure of the electron energy then t can be obtained from experimental data. Frost and Phelps [12] define the corresponding collision frequency as the "energy exchange collision frequency". The quantity tn is a function of E/n. The calculated energy relaxation times for CH_4 at the high E/n values which are typical of RF deposition discharges are typically a few ns, short compared with the RF period. Therefore, time and space averaged electron excitation and dissociation rates can be used in rate equation models in order to predict the chemical kinetic processes which are active during film deposition.

For the plasma conditions of 300 mtorr, 30sccm flow, and 20W RF power, the electric field was determined from the measured peak-to peak RF voltage divided by the 2 cm electrode spacing. The measured peak E/n value is about 5000 Townsends. This leads to an average value of about 1800 Townsends based on our waveforms, which corresponds to k_i and k_d values that are about equal at 5.5(10)-8 cm3/sec as seen in Figure 7. These values are used as estimates of the time and space averaged values of k_i and k_d in the chemical kinetics calculations. Dissociation and ionization are the dominant electron energy loss channels. Therefore:

$$\text{Power/Volume} = k_d n_e \, n\varepsilon_d + k_i \, n_e n\varepsilon_i$$

and we estimate the average electron density:

$$n_e = 1.4(10)^8 \text{ cm}^{-3}$$

From solutions of:

$$dn/dt = -(k_d + k_i)\, n_e$$

we find that the methane density, n, is reduced to about 45% its initial value after the 0.1 second residence time of the reactant in the plasma. Experimentally we find the methane density to be 75% of its initial value, a significant difference between theory and experiment. We will see in the following section that consideration of the chemical kinetics of the dissociated species can reduce this discrepancy via homogeneous recombination reactions.

CHEMICAL KINETICS MODELLING

The time and space averaged densities of various charged and neutral species in the discharge were estimated by solving rate equations of the type:

$$\frac{dn_i}{dt} = \gamma_{pj}\, n_e - \frac{D_j}{\Lambda_j^2}\, nj - k_{rij}\, n_i n_j$$

where the γ_{pj} are production rates due to electron-molecule collisions, $(D_j/\Lambda_j^2)n_j$ are diffusion loss rates, and $k_{rij} n_i n_j$ are reaction loss terms. These "plug flow reactor" equations follow the species densities in a volume element of gas as it flows through the reactor. The rate equations are solved using the numerical method of Gear [13] and the computer code of Reference 10.

The electron impact collision rates were estimated by assuming:

$$\gamma_{pj} = k_{pj}\, n = f\,(E_{avg}/n)\, n$$

The rate coefficients for the electron collision reactions are obtained from the results of the electron kinetics calculations discussed above.

The diffusion loss rates were estimated by using a formulation developed by Chantry [14]. It takes reflection at the boundaries into account by deriving an effective diffusion length which increases as the reflection coefficient at the boundaries increases. The "extrapolated diffusion length" [15] given by:

$$\frac{1}{n}\frac{dn}{dx} = -\frac{1}{\lambda}$$

is the basis for this formulation. When the discharge region is bounded by parallel planes the extrapolated diffusion length for species j is given by:

$$\lambda_j = \frac{2D_j(1+R)}{v_j(1-R)}$$

where D_j is the diffusion coefficient, v_j is the mean velocity, and R is the reflection coefficient (1 minus the sticking coefficient). The boundary

condition is discussed in detail by Chantry et al [16]. The corresponding effective diffusion length is given by:

$$\frac{1}{\Lambda_j^2} \quad \frac{1}{\Lambda_0^2 + \ell_0 \lambda_j}$$

where $\Lambda_0 = d/\pi$ is the conventional diffusion length, ℓ_0 is the ratio of the discharge volume to its wall area. The diffusion rates were estimated by using the known ion mobilities in the expression:

$$Dn = \mu n \, (kT_i/e)$$

where k is the Boltzmann constant, T_i is the ion temperature which is assumed to be the same as the gas temperature, and e is the electronic charge. Sticking coefficients are not known for the species of interest here, but their values strongly affect the net diffusion losses to the walls (deposition rates). Several authors [5,17] have suggested that sticking coefficients can be less than unity. In fact, for high coverages as we have in our deposition experiments, very low values may be reasonable for some species [18]. Processes other than simple reflection must also be considered, including the entire set of dissociative chemisorption processes that result in heterogeneous reaction products returning to the plasma, and charge neutralization of ionized species. These processes and their rates are known to depend upon fluxes and energies of the ions incident upon the surface. We have performed the chemical kinetics calculations handling these diffusion losses in several different ways in order to elucidate the chemical reaction paths in the plasma. The comparisons are made to the same set of experimental conditions that we discussed above in the section on electron kinetics calculations. Space is not available in this article to discuss all of the reactions and chemical kinetics data that went into the calculations. Another publication is planned for the near future to deal with these topics more completely.

Results And Comparison To Experiments

We will first describe a model based on a set of assumed surface reactions that lead to results reasonably close to those observed experimentally. We will then discuss how the predictions of the model are changed when different surface reactions are used. This model is illustrated schematically in Figure 8, showing the methane dissociation and the main reaction paths leading to deposition, recombination, and production of stable gaseous products in the downstream gases. The predictions of species densities and deposition rates of this model agree with experimental measurements to within about a factor of two. For this case we assumed a sticking coefficient of unity for CH_3^+ and 0.02 for CH_3, other ions are assumed only to neutralize at the walls, and no other surface reactions were considered. It can be seen that CH_3 is the key intermediate radical in one of the deposition paths and in the production of the stable products, C_2H_6 and C_2H_4. Not obvious from the diagram is the fact that most of the CH_3 is produced from CH_3^+ via the cycle which includes $C_2H_5^+$ and C_2H_5. The higher the sticking coefficient of CH_3^+, the better the agreement with the experiments, hence unity was used. CH_3 was chosen to have non-zero sticking coefficient because it results in uniform deposition rates as we observe experimentally. The value of 0.02 yields a rate that agrees with experiments. We probably could have fit the data nearly as well by assuming

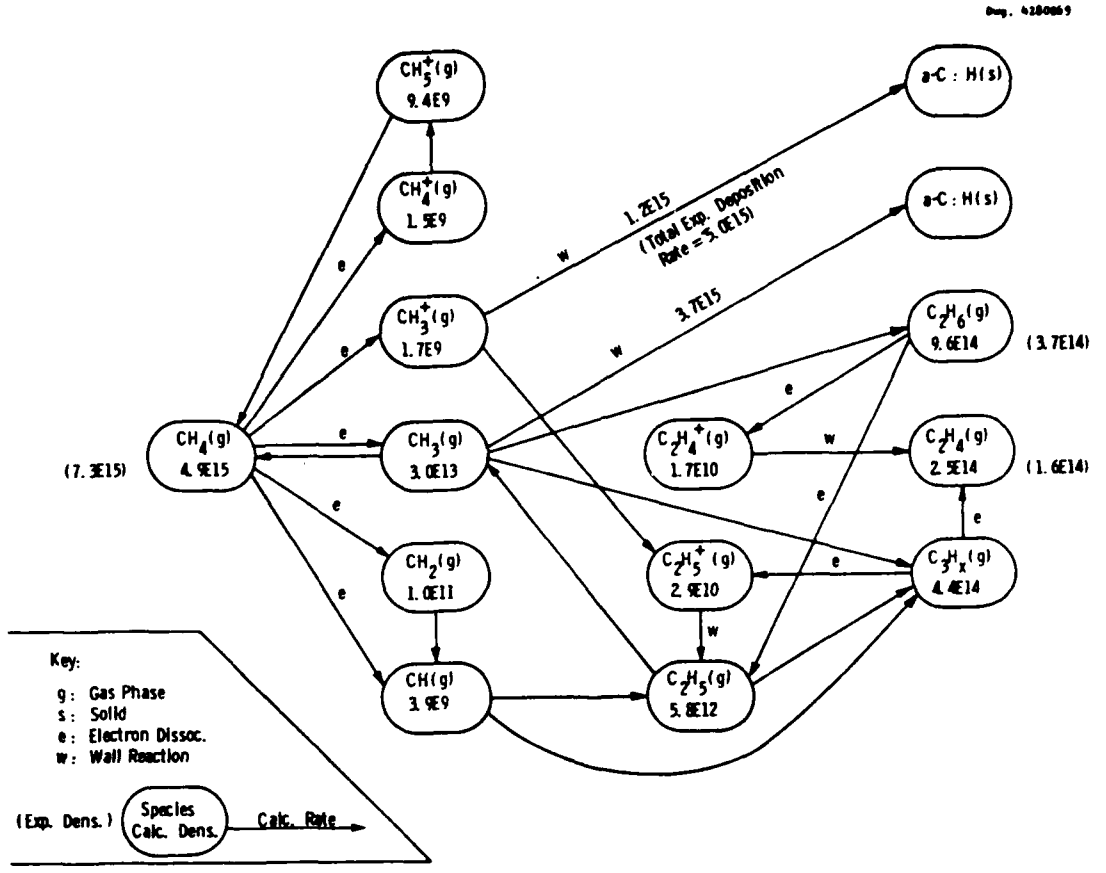

Figure 8. Schematic diagram of the chemical kinetic paths in the methane plasma for assumed surface reactions leading to realistic prediction.

non-zero sticking coefficient for $C_2H_5^+$, but deposition would not have been as uniform. Other reactive species were found to have deposition rates with much stronger dependence upon position, or were present in such small quantities that deposition would be insignificant even if unit sticking coefficients were assumed. These findings are summarized in Table I, obtained for a case that was calculated assuming unit sticking coefficients for all reactive species present in significant quantities. Here the model predicted far too much deposition and not enough stable stable gas products. Other cases were run to help us sort out the important processes. When homogeneous ion-molecule reactions were excluded from the calculation, for example, a lower net dissociation of methane was seen, comparable to experiments, but deposition rates and product species were much too low.

Conclusions

We have developed a model which is capable of treating the important physical and chemical processes leading to the deposition of carbon films. Even though the mass transport rates in the deposition reactions amounts to only a few percent of the reactant flow rates in this example, their influence on the gas phase chemistry is much greater. This is probably valid in any practical set of conditions used for deposition.

Comparison of the model to experiments leads us to conclude that the most likely species involved in the deposition processes are CH_3^+, CH_3, and $C_2H_5^+$ in that order. There is good evidence for excluding other radicals and ions as major contributors to deposition. Our best case model uses

TABLE I

Deposition Rates for Reactive Species when Unity Sticking Coefficients are Assumed.

Model Predictions:		
Species	Deposition Rate	Spatial Distribution
CH_2	$4.6(10)^{12}$	Uniform
CH^2	$6.6(10)^{12}$	Less Uniform
C_2H_5	$3.0(10)^{13}$	Less Uniform
CH_3^+	$1.1(10)^{15}$	Uniform
CH_3	$2.0(10)^{15}$	Uniform
$C_2H_5^+$	$9.1(10)^{15}$	Less Uniform
CH_5^+	$1.8(10)^{16}$	Non-Uniform
Exparimental Deposition:	$5.0(10)^{15}$	Uniform

sticking coefficients of 1.0 and 0.02 for CH_3^+ and CH_3 respectively. Our mass transport data show a strong dependence of deposition rates on the plasma sheath potential.

We would like to see independent determinations made of the individual surface reaction rates, for example, with radical ion beams. This would greatly reduce the amount of estimating needed to make predictions with the model.

ACKNOWLEDGMENTS

The authors would like to acknowledge the technical assistance of R. A. Madia in the experimental measurements, of W. Petlevich for digitizing the RF waveforms, and to A. Wolfe for the microbalance measurements. Helpful technical discussions with P. J. Chantry are gratefully acknowledged.

REFERENCES

1. Makoto Hayashi, 6th Symposium on Dry Process, Tokyo, Japan, October, 1984.

2. Laurence E. Kline, IEEE Transactions on Plasma Science PS-10, No. 4, 224 (1982).

3. W. Tsang and R. F. Hampson, "Chemical Kinetics Data Base for Methane Combustion", NBS Report NBSIR-84-2913, (1984).

4. D. L. Albritten, Atomic Data and Nuclear Tables 22, 1 (1978).

5. K. Tachibana, M. Nishida, H. Harima, and Y. Urano, J. Phys. D: Appl. Phys 17, 1727 (1984); K. Tachibana, T. Okuyama, H. Harima, and Y. Urano, Int'l Symposium on Plasma Chemistry, Eindhoven, July, 1985.

6. Brian Chapman, "Glow Discharge Processes", (John Wiley & Sons, New York, 1980), p.53, 69.

7. Y. Catherine, P. Couderc, and B, Grolleau, 7th International Symposium on Plasma Chemistry, Endhoven, The Netherlands, July, 1985.

8. R. A. Gottscho and M. L. Mandich, J. Vac. Sci. Tech. (To be published).

9. S. D. Rockwood, Phys. Rev. A8, 2348 (1973).

10. W. B. Lacina, "Theoretical Modeling of Molecular and Electronic Kinetic Processes", Final Report, Office of Naval Research Contract No. N00014-78-0499, Jan. 1979.

11. L. E. Kline, to be published (IEEE Transactions on Plasma Science, 1986).

12. L. S. Frost and A. V. Phelps, Phys. Rev. 127, 1621 (1962).

13. C. W. Gear, "Numerical Initial Value Problems in Ordinary Differential Equations", (Prentiss-Hall, Englewood Cliffs, NJ, 1971).

14. P. J. Chantry, (private communication).

15. E. W. McDaniel, "Collisional Phenomena in Ionized Gases", (Wiley, New York, 1964).

16. P. J. Chantry, A. V. Phelps, and G. J. Shultz, Phys. Rev. 152, 81 (1966).

17. D. Edelson and D. Flamm, J. Appl. Phys. 56, 1522 (1984).

18. C. T. Rettner, H. E. Pfnur, and D. J. Auerbach, Phys. Rev. Lett. 54, 2716 (1985).

REFERENCE 2

J. Appl. Phys.
Date: 25 March 1986

REACTION CHEMISTRY AT THE Si(100) SURFACE - CONTROL THROUGH ACTIVE SITE MANIPULATION

M. J. Bozack, W. J. Choyke[a,b], L. Muehlhoff[a], and J. T. Yates, Jr.

Surface Science Center
Department of Chemistry
University of Pittsburgh
Pittsburgh, PA 15260

[a] Department of Physics, University of Pittsburgh, Pittsburgh, PA

[b] Westinghouse Research & Development Center, Pittsburgh, PA

REACTION CHEMISTRY AT THE Si(100) SURFACE - CONTROL THROUGH ACTIVE SITE MANIPULATION

M. J. Bozack, W. J. Choyke[a,b], L. Muehlhoff[a],

and J. T. Yates, Jr.

Surface Science Center
Department of Chemistry
University of Pittsburgh
Pittsburgh, PA 15260

ABSTRACT

Thermal desorption methods have been used to investigate the interaction of propylene (C_3H_6) with Si(100)-(2 X 1). The adsorption characteristics depend strongly on the availability of active sites at the Si(100) surface. Reactivity is enhanced by production of active sites during ion prebombardment. Adsorption of C_3H_6 to a disordered, ion bombarded Si(100) surface results in nearly complete dissociation of C_3H_6 for current densities as small as 10^{15} Ar^+ ions/cm^2. In contrast, for a thermally annealed and ordered Si(100) surface, only ~ 60% of the C_3H_6 dissociates. The remainder of the propylene chemically bonds to the surface as an undissociated molecule which desorbs intact at 550 K. The increase in reactivity is due to an increase in dissociative chemisorption which occurs at defect sites produced by ion bombardment. Reactivity is suppressed by capping of

[a] Department of Physics, University of Pittsburgh, Pittsburgh, PA
[b] Westinghouse Research & Development Center, Pittsburgh, PA

REFERENCE 2

J. Appl. Phys.
Date: 25 March 1986

REACTION CHEMISTRY AT THE Si(100) SURFACE - CONTROL THROUGH ACTIVE SITE MANIPULATION

M. J. Bozack, W. J. Choyke[a,b], L. Muehlhoff[a], and J. T. Yates, Jr.

Surface Science Center
Department of Chemistry
University of Pittsburgh
Pittsburgh, PA 15260

[a] Department of Physics, University of Pittsburgh, Pittsburgh, PA

[b] Westinghouse Research & Development Center, Pittsburgh, PA

REACTION CHEMISTRY AT THE Si(100) SURFACE - CONTROL THROUGH ACTIVE SITE MANIPULATION

M. J. Bozack, W. J. Choyke[a,b], L. Muehlhoff[a],

and J. T. Yates, Jr.

Surface Science Center
Department of Chemistry
University of Pittsburgh
Pittsburgh, PA 15260

ABSTRACT

Thermal desorption methods have been used to investigate the interaction of propylene (C_3H_6) with Si(100)-(2 X 1). The adsorption characteristics depend strongly on the availability of active sites at the Si(100) surface. Reactivity is enhanced by production of active sites during ion prebombardment. Adsorption of C_3H_6 to a disordered, ion bombarded Si(100) surface results in nearly complete dissociation of C_3H_6 for current densities as small as 10^{15} Ar^+ ions/cm^2. In contrast, for a thermally annealed and ordered Si(100) surface, only ~ 60% of the C_3H_6 dissociates. The remainder of the propylene chemically bonds to the surface as an undissociated molecule which desorbs intact at 550 K. The increase in reactivity is due to an increase in dissociative chemisorption which occurs at defect sites produced by ion bombardment. Reactivity is suppressed by capping of

[a] Department of Physics, University of Pittsburgh, Pittsburgh, PA
[b] Westinghouse Research & Development Center, Pittsburgh, PA

active sites using atomic hydrogen preadsorption. Hydrogen passivates the Si(100) surface by occupation of silicon dangling bonds, which prevents adsorption of C_3H_6. By controlling the number and kind of active surface sites in this way, it is possible to manipulate the reactive ability of the Si(100) surface.

I. INTRODUCTION

The ability to control the reaction of gas-phase hydrocarbons with semiconductor surfaces forms the basis for several technological processes. Chemical vapor deposition (CVD), plasma vapor deposition (PVD), reactive ion etching (RIE), and epitaxial growth all depend upon the ability of molecules to react with a surface. There has been limited understanding of these processes due to the high pressures involved and the lack of controls in a typical plasma reactor. A number of studies have shown that deposition and etch rates have been increased by energetic particle bombardment of the surface during exposure to reactive gases [1-5]; however, it has been difficult to determine which step in the process (adsorption, product formation, or desorption) is directly affected by the irradiation. Our interest in examining propylene on Si(100) is to obtain a better understanding of the reactivity of Si toward this class of hydrocarbon molecules. This system has a direct connection to SiC thin film formation in CVD and PVD processes.

II. EXPERIMENTAL PROCEDURES

The experiments were performed in an ion-pumped, stainless steel UHV system equipped with a scanning Auger spectrometer, a quadrupole mass spectrometer, and a plasma discharge ion source. The ion source was used for in situ cleaning and ion irradiation of the Si(100) surface, and possessed rastering and focusing capabilities. The angle of incidence of the ion beam with respect to the surface normal was 70 degrees. Surface cleanliness was verified by Auger spectroscopy. Thermal desorption spectra were recorded digitally with a multiplexed, computer-driven mass spectrometer system which could record several mass peaks simultaneously. Integration of the desorption spectra and linear background subtraction were performed through software routines. The temperature ramp for thermal desorption was provided by a focused 900 W tungsten-halogen lamp. The temperature ramp was nonlinear but highly reproducible. Propylene was delivered to the Si(100) surface by using a precision tubular molecular beam doser. The flow rate from the doser was controlled by a 2.6 micron diameter orifice inside the doser assembly. The flux rate was 2.4×10^{14} molecules/torr-sec, varied by adjustment of backing pressure and time. The on/off characteristic of the doser approximated a square pulse with a sharp leading edge. A heated circular loop of 20 mil W wire served as a source for atomic hydrogen by molecular dissociation of $H_2(g)$ to $2H(g)$. Due to the unknown H(g) arrival rate at the Si(100) surface, we specify the exposure in Langmuirs (1 L = 10^{-6} torr-sec) of the constant

background $H_2(g)$ pressure used and the time of exposure. The filament temperature was 2100 K and the sample-emitter distance was 2 cm during the exposure. The Czochralski grown silicon was B-doped, p-type material of 10 ohm-cm resistivity. The base material was oriented by Laue back reflection (±1°), and Si(100) slices were cut and polished into specimens 1.5 cm x 1.5 cm x 0.17 cm thick. These were cleaned prior to insertion into the chamber using standard degreasing/oxidation/HF cleaning procedures.

III. RESULTS AND DISCUSSION

A. Active Surface Sites on Clean, Ordered Si(100)

Investigation of the bonding and reactivity of C_3H_6 with Si(100) using temperature programmed desorption (TPD) techniques is shown in Figure 1. The surface was prepared by 2 kV Ar^+ sputter cleaning, followed by high temperature annealing in vacuum. The annealing was carried out at a temperature of 1075 K for about 5 minutes. Studies by Bean et al. [6] have shown that a well-ordered Si(100)-(2 X 1) surface is recoverable by this procedure.

The propylene adsorption was carried out at a temperature of 130 K. Two desorption peaks are observed: a weaker binding state of large population at about 550 K, and a stronger binding state of low relative population at about 590 K. The stronger binding state is evident only at low coverages of propylene; at higher

coverages, it is lost in the trailing edge of the weaker bound state. The observation of an intact propylene molecule desorbing at such high temperatures on Si(100) is somewhat surprising, and points to the establishment of a rather strong Si-C_3H_6 surface bond which probably forms at the C=C molecular site in the molecule. Calculation of the desorption energy and preexponential factor were made assuming first-order kinetics. Following the analysis of Chan et al. [7], the desorption energy was calculated to be 1.2 eV and the preexponential factor was found to be 9.3×10^9 s^{-1}.

Only ~ 40% of the adsorbed propylene remains intact during adsorption and can be liberated by thermal desorption. The remainder undergoes dissociation. This was shown by measuring the C/Si Auger ratio before and after thermal desorption. Throughout the range of coverages, ~ 60% of the carbon that was adsorbed remained on the surface in the form of a carbon-containing overlayer (See Figure 2). There are thus two reaction pathways for C_3H_6 on Si(100). In one pathway, propylene chemically bonds to Si(100) as an undissociated molecule which desorbs intact. In the other pathway, propylene dissociatively chemisorbs to fragments of unknown character. Examination of other molecular species likely to desorb as a result of fragmentation was negative; in particular, no $H_2(g)$ was observed above the background hydrogen signal.

B. Enhancement of Reactivity by Active Site Production

The effect of surface defects on the thermal desorption of C_3H_6 on Si(100) is shown in Figure 3. In this experiment, the

silicon surface was prebombarded with a rastered, defocused beam of Ar^+ ions at an accelerating potential of 2.0 kV. A constant dose of 1.2×10^{14} propylene molecules per square centimeter was then added to the damaged surface. By performing the ion irradiation before adsorption, we are able to separate the effect of surface defect enhancement of reactivity from other processes such as ion-induced dissociation of adsorbed layers and free radical production in the gas phase.

The resulting desorption curves show that increased surface disorder results in enhanced chemical reactivity. This is demonstrated by the reduction in the propylene desorption yield with increasing fluences of prebombarding Ar^+ ions. The reduction in propylene desorption yield is characterized in Figure 4. It is observed that little change in silicon surface chemistry occurs for Ar^+ current densities below 10^{12} ions/cm^2. For additional prebombardment, however, the desorption yield falls steadily to an asymptotic, near-zero value which is reached when about 10^{15} ions/cm^2 have collided with the surface. The fact that such small ion current densities affect the surface chemistry has fundamental implications for PVD and RIE processes, which are typically performed under conditions of high pressure and high ion bombardment rates. It is possible to calculate a damage cross section for the production of surface Si defects by ion bombardment [8]. Here we use the relative concentration of <u>undecomposed</u> C_3H_6 as an index of the fraction of <u>undamaged</u> Si surface sites. For the concentration of undamaged C_3H_6 species

at the surface, N(t),

$$N(t) = N_o \exp(-IQt/Ae) \qquad (1)$$

where N_o is the initial undamaged C_3H_6 concentration (molecules/cm^2), I is the total ion current, A is the irradiated area, t is the time, and e is the electronic charge, 1.6×10^{-19} coulombs. Q is the effective cross section for the surface defect-stimulated decrease in $N(t)/N_o$. Thus Q is a measure of the cross section for the Si(100) damage by Ar^+ as detected by chemical means. Using values for N taken from the desorption peak areas in Figure 4, the damage cross section for 2 kV Ar^+ ions is 2.7×10^{-15} cm^2 [9]. The points were fitted by a least squares exponential with a coefficient of determination of 0.81 (perfect fit = 1.00).

C. Suppression of Reactivity by Active Site Capping

Preadsorbed hydrogen acts to prevent propylene adsorption by occupation of potential adsorption sites. The effect is shown in Figure 5. Varying preexposures of atomic hydrogen were adsorbed onto a clean, annealed face of Si(100), followed by addition of a constant dose (1.2×10^{14} molecules/cm^2) of C_3H_6. The overlayer was then desorbed in the usual fashion. The resulting desorption curves show that higher preexposures of H result in lower propylene desorption yields. The desorption peak is also observed to shift to higher temperatures. It appears that the weak C_3H_6

binding state near 550 K is influenced more by the H underlayer than the stronger C_3H_6 binding state at 590 K. The reduction in desorption yield is due to a reduction in the propylene adsorptive capacity rather than an increase in molecular dissociation at the surface. In other words, fewer molecules of propylene have desorbed because fewer have adsorbed on the H-capped Si surface. This was shown by investigation of the mass spectrometer signal for C_3H_6 during adsorption, which showed that higher preexposures to hydrogen resulted in lower propylene uptake by the Si(100) surface. Hydrogen, therefore, acts to suppress the reaction between C_3H_6 and Si(100) by capping of dangling Si surface sites. Once occupied, the bonding sites are unable to combine with propylene and the surface is rendered passive to further chemical reaction.

D. The Range of Active Site Manipulation

The range over which Si(100) surface reactivity may be altered by surface defect site production and H-capping has implications for CVD and RIE processes. A pertinent question is whether the two effects described above can be played against one another. For example, can the active sites produced by ion bombardment be subsequently capped by hydrogen adsorption?

The answer is yes, as shown by the following experiment: (1) a heavily disordered Si(100) surface was prepared by prebombardment with $> 1.0 \times 10^{15}$ Ar^+/cm^2; (2) the disordered surface was exposed to varying amounts of atomic hydrogen; (3) a constant

dose of 1.2×10^{14} C_3H_6 molecules per cm^2 was added to the surface; and (4) the overlayer was desorbed in the normal fashion. Step 3 was monitored by the mass spectrometer to characterize the reflected flux of propylene by the crystal. This was done because no propylene desorption was observed: for a fully disordered surface, no desorption was observed because propylene dissociates on adsorption; for a fully capped surface, no desorption was observed because no propylene adsorbs; for an intermediate case, no desorption was observed because some of the incident propylene dissociates and the rest does not adsorb.

The propylene uptake by the damaged Si(100) surface after various exposures to hydrogen is shown in Figure 6. In this figure, the reflection of C_3H_6 from the Si(100) face as seen by the mass spectrometer is recorded during propylene adsorption. When a typical dose of C_3H_6 is applied to a clean Si(100) crystal, the reflected signal approximates a square pulse with a sharp leading edge, shown by curve d at low H exposures. The flat plateau in the reflected C_3H_6 signal indicates a constant sticking coefficient during adsorption. Termination of uptake by the crystal is indicated by a gradual rise in the mass spectrometer signal at the end of the adsorption plateau, as a larger fraction of the incident molecules are reflected.

It is readily observed that the C_3H_6 uptake decreases for larger exposures to hydrogen. This indicates a loss of available adsorption sites, and shows that the active sites produced by ion

bombardment may be capped by hydrogen adsorption. For low exposures (~ 1 L), there is little effect on propylene uptake. For exposures above ~ 10 L, however, C_3H_6 uptake occurs for only a brief interval after the doser is turned on. This indicates that the adsorptive capacity for propylene on the ion bombarded surface is decreasing with larger H exposures. Auger examinations of the surface support this view, as higher exposures of the disordered surface to atomic hydrogen is accompanied by decreasing surface concentrations of C produced by dissociation of C_3H_6.

IV. CONCLUSIONS

The reaction of propylene with Si(100) occurs via two simultaneous pathways. In the first, propylene bonds to the silicon surface as an undissociated molecule which desorbs intact at a temperature of ~ 550 K with a desorption activation energy of ~ 1.2 eV. In the second, propylene dissociatively chemisorbs to fragments of unknown character. By manipulation of active sites, it is possible to control the degree of chemical reaction at the surface. Reaction is promoted by production of active defect sites during ion prebombardment. Reaction is suppressed by removal of active sites by hydrogen capping. By manipulating the degree of ion bombardment and hydrogen adsorption, the effects may be played against each other to produce a full range of reactive chemistry on Si(100). That silicon surface chemistry

is directly influenced by formation of surface defects has significance for processes of CVD and RIE.

ACKNOWLEDGEMENTS

The authors acknowledge the support of this work under AFOSR Contract No. F49260-84-C-0063DEF.

REFERENCES

1. J. W. Coburn and H. F. Winters, J. Vac. Sci. Technol. 16(2), 391 (1979).

2. J. W. Coburn and H. F. Winters, J. Appl. Phys. 50(5), 3189 (1979).

3. J. Dieleman, F. H. M. Sanders, A. W. Kolfschoten, P. C. Zalm, A. E. de Vries, and A. Haring, J. Vac. Sci. Technol. B. 3(5), 1384 (1985).

4. U. Gerlach-Meyer, J. W. Coburn, and E. Kay, Surf. Sci. 103, 177 (1981).

5. E. Ikawa, K. Noguchi, and Y. Kurogi, Proc. Int'l Ion Engineering Congress, ISIAT '83 and IPAT '83, 1517 (1983).

6. J. C. Bean, G. E. Becker, P. M. Petroff, and T. E. Seidel, J. Appl. Phys. 48(3), 907 (1977).

7. C. M. Chan, R. Aris, and W. H. Weinberg, Appl. Surf. Sci. 1, 360 (1978).

8. T. E. Madey and J. T. Yates, Jr., J. Vac. Sci. Technol. 8, 525 (1971).

9. M. J. Bozack, W. J. Choyke, L. Muehlhoff, and J. T. Yates, Jr., submitted.

FIGURE CAPTIONS

Fig. 1 C_3H_6 thermal desorption spectra from clean, annealed Si(100). The existence of active surface adsorption sites are indicated with a binding energy for C_3H_6 of ~ 1.2 eV.

Fig. 2 Comparison of the C/Si AES peak ratio before and after thermal desorption. About 60% of the adsorbed C_3H_6 has dissociated.

Fig. 3 C_3H_6 thermal desorption spectra from disordered Si(100) for increasing Ar^+ prebombardment. The decrease in desorption yield for increasing Ar^+ current indicates an enhancement of reactivity by active site production.

Fig. 4 C_3H_6 thermal desorption peak area from Si(100) vs. prebombarding Ar^+ current density. The peak areas were calculated from the data of Fig. 2. (Inset) Calculation of the cross section for the production of surface defects on Ar^+ bombarded Si(100). The cross section is 2.7×10^{-15} cm^2.

Fig. 5 C_3H_6 thermal desorption spectra from ordered Si(100) vs. preadsorbed H exposure. The desorption yield decreases with H coverage due to site capping, which suppresses the amount of propylene which can be adsorbed.

Fig. 6 Reflected C_3H_6 signal from heavily damaged Si(100) *vs.* preadsorbed H exposure. The sites created by the ion bombardment are subsequently capped by H adsorption, resulting in lower propylene uptake by the crystal.

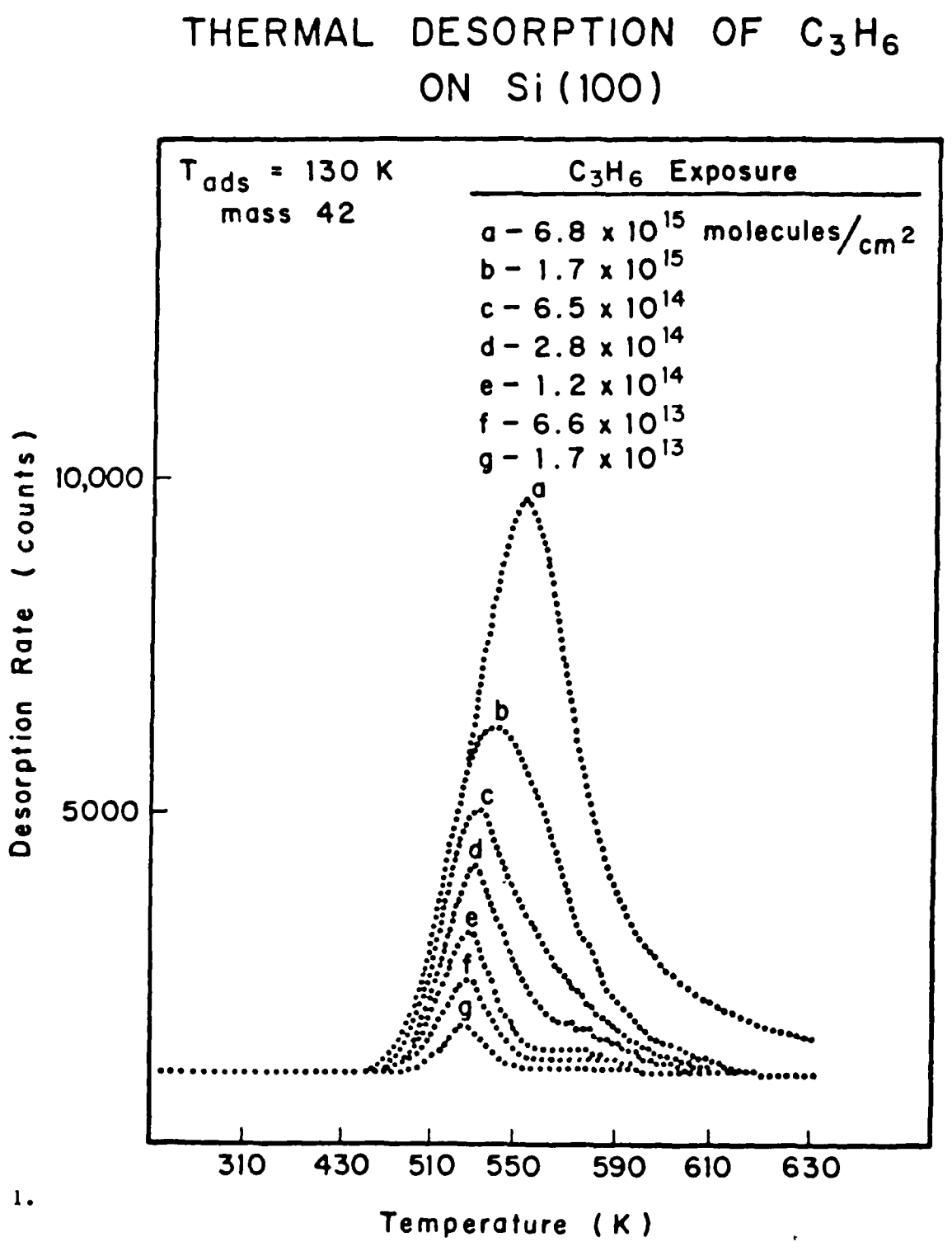

Figure 1.
Bozack
Choyke
Muehlhoff
Yates

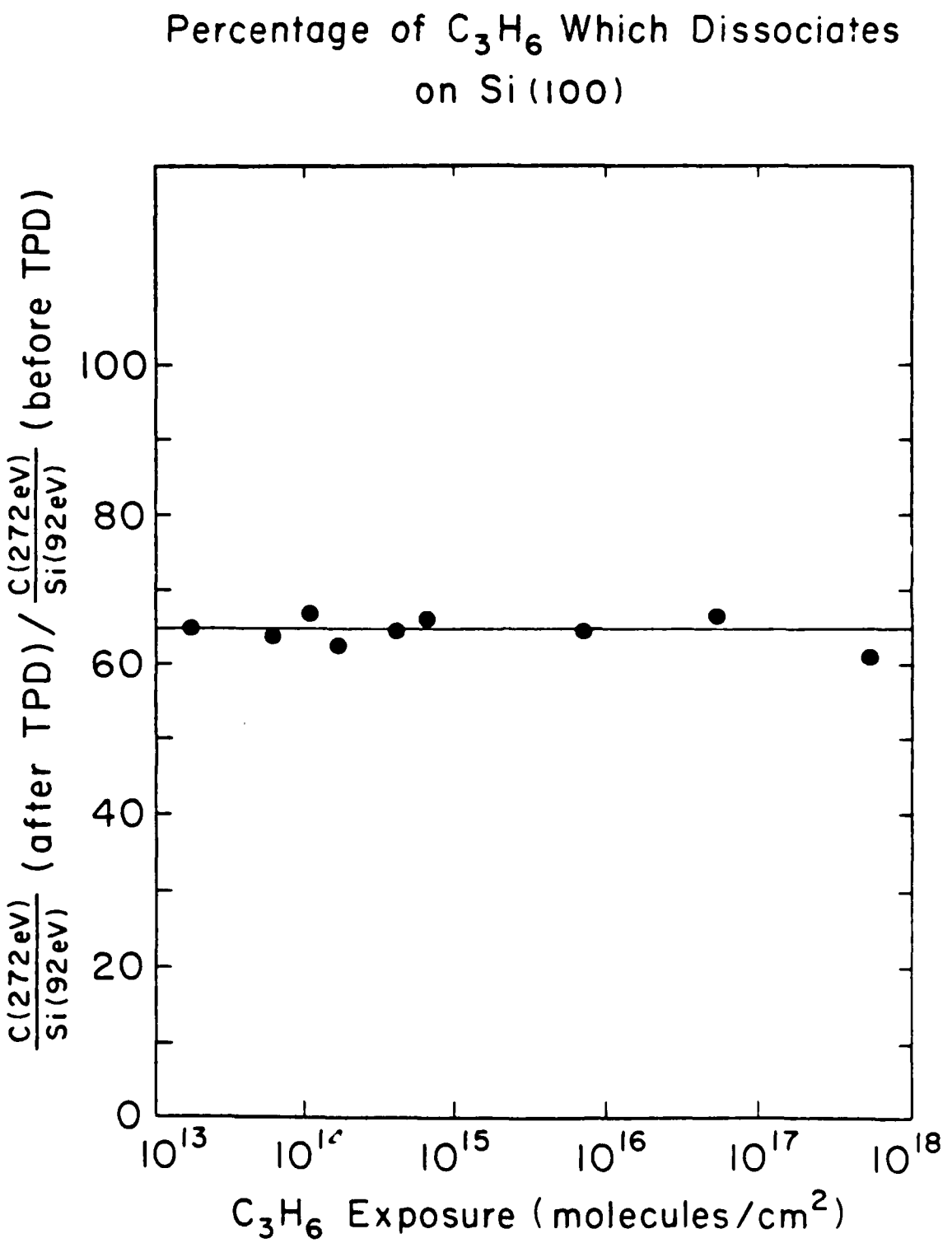

Figure 2.
Bozack
Choyke
Muehlhoff
Yates

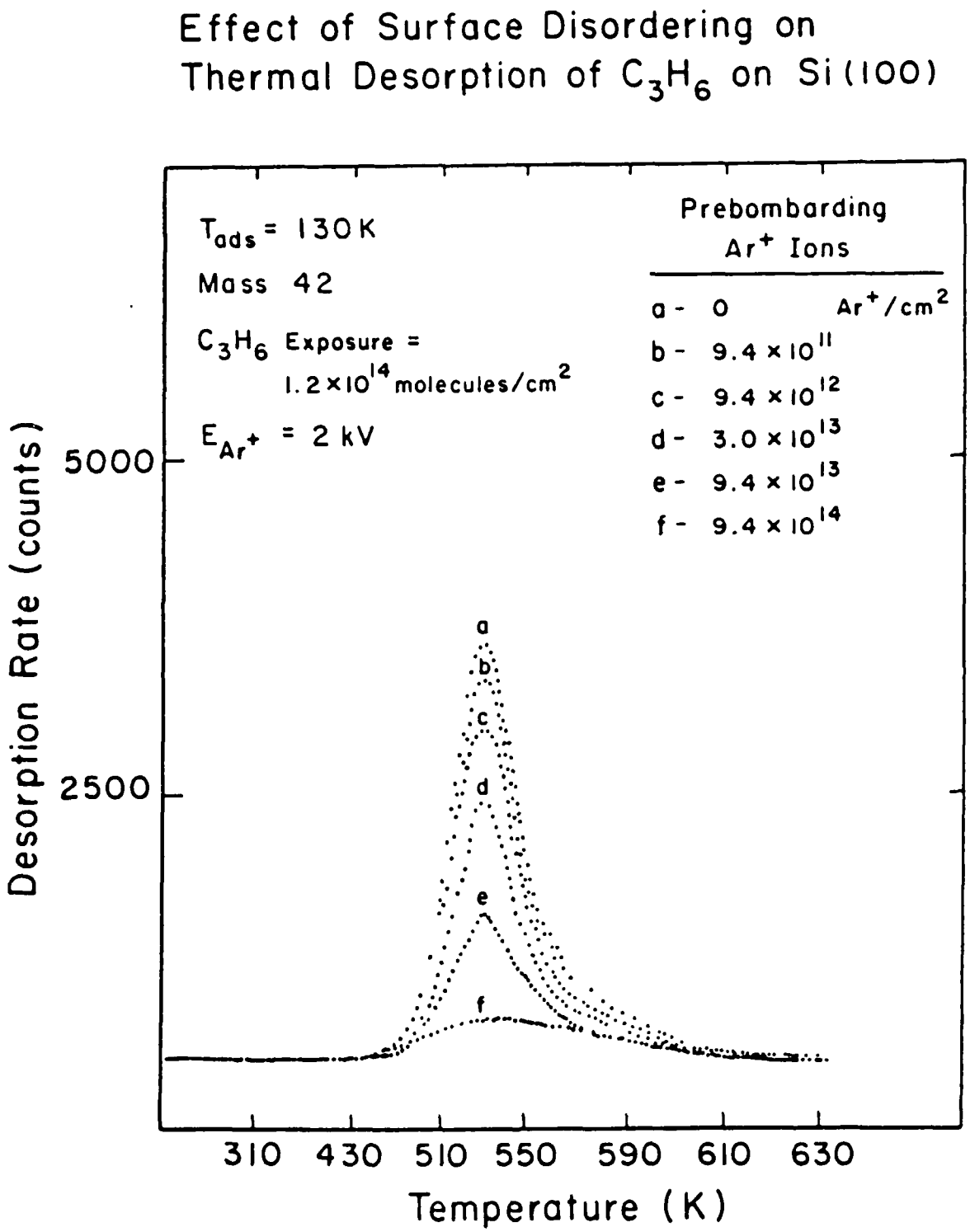

Figure 3.
Bozack
Choyke
Muehlhoff
Yates

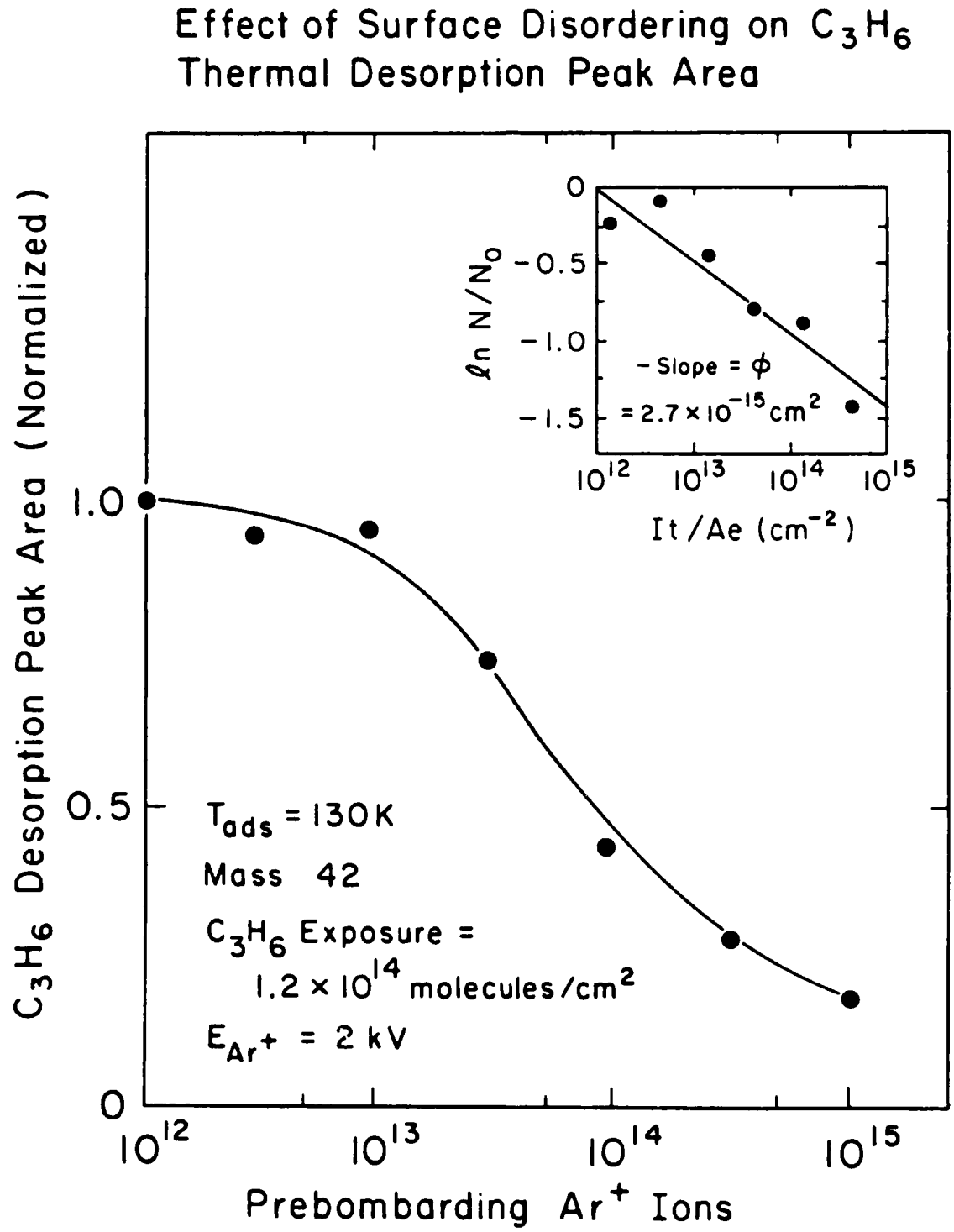

Figure 4.
Bozack
Choyke
Muehlhoff
Yates

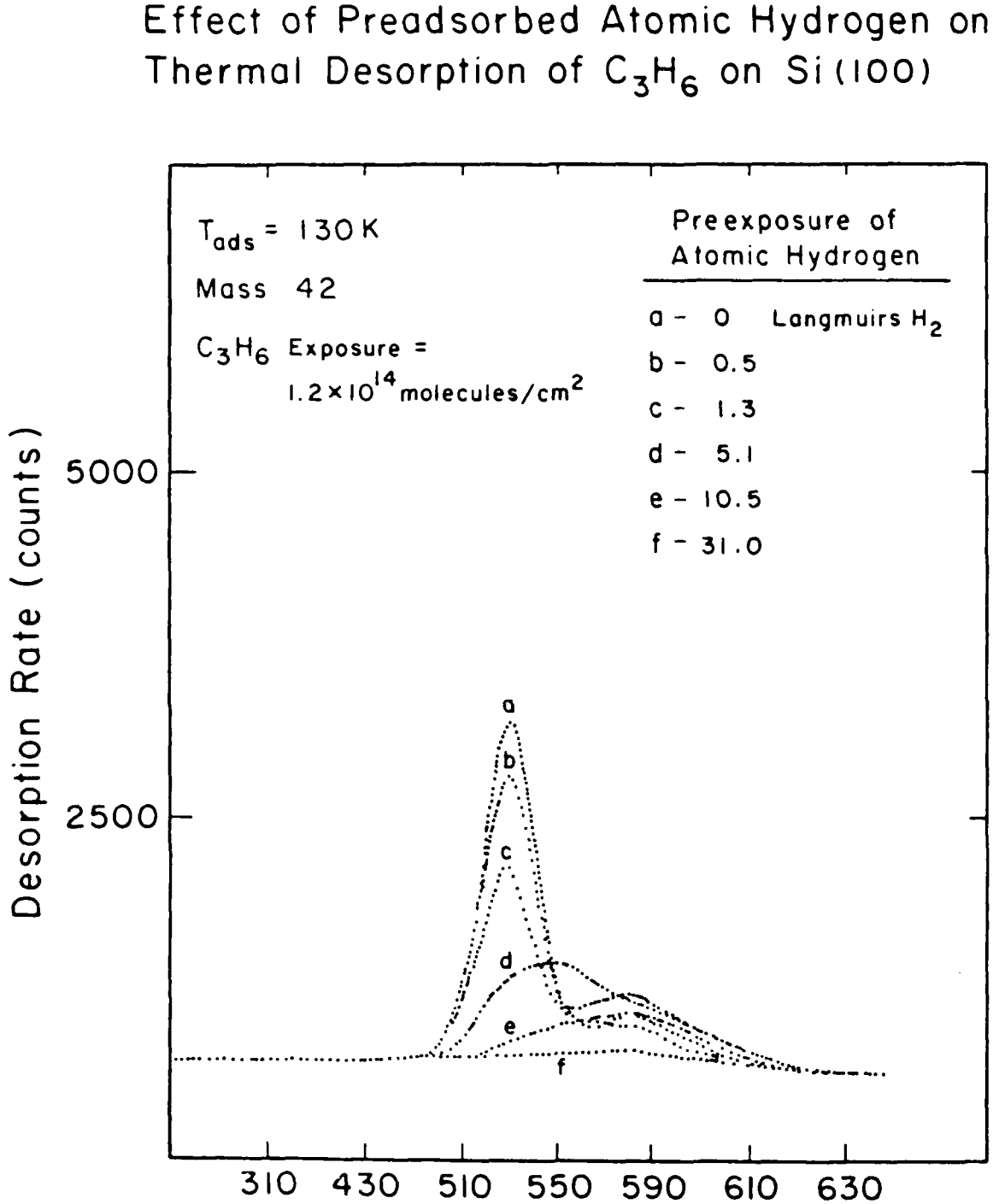

Figure 5.
Bozack
Choyke
Muehlhoff
Yates

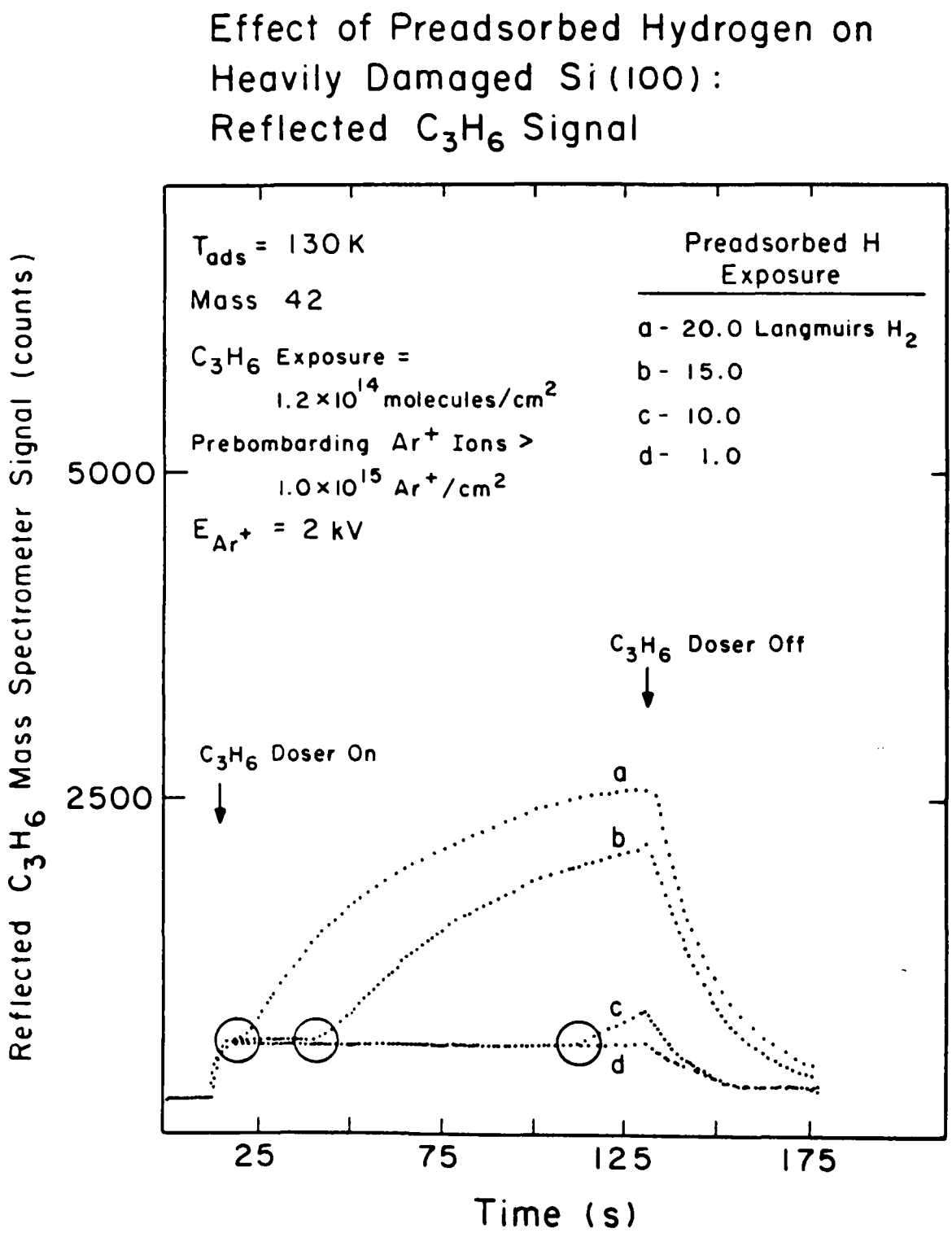

Figure 6.
Bozack
Choyke
Muehlhoff
Yates

REFERENCE 3

J. Vac. Sci. Tech.
Date: 26 March 1986

METHODS IN SEMICONDUCTOR SURFACE CHEMISTRY

M. J. Bozack, L. Muehlhoff[a], J. N. Russell, Jr.

W. J. Choyke[a,b], and J. T. Yates, Jr.

Surface Science Center
Department of Chemistry
University of Pittsburgh
Pittsburgh, Pennsylvania 15260

[a] Department of Physics, University of Pittsburgh, Pittsburgh, PA

[b] Westinghouse Research & Development Center, Pittsburgh, PA

METHODS IN SEMICONDUCTOR SURFACE CHEMISTRY

M. J. Bozack, L. Muehlhoff[a], J. N. Russell, Jr.
W. J. Choyke[a,b], and J. T. Yates, Jr.

Surface Science Center
Department of Chemistry
University of Pittsburgh
Pittsburgh, Pennsylvania 15260

ABSTRACT

Methods for studying semiconductor surface chemistry are presented. It is shown that adsorption and desorption kinetic measurements, when combined with Auger spectroscopy, can give useful insights into fundamental elementary surface kinetic processes which are important in understanding the behavior of complex CVD, PVD, or RIE processes. Techniques for crystal preparation, mounting, temperature control, and reaction kinetic measurements are given using examples from the adsorption and reaction of propylene with Si(100). An illustration of the manipulation of active site availability on Si(100) is described.

[a] Department of Physics, University of Pittsburgh, Pittsburgh, PA
[b] Westinghouse Research & Development Center, Pittsburgh, PA

I. INTRODUCTION

The surface chemistry which occurs on semiconductor surfaces is of fundamental importance to many semiconductor technologies. Processes of chemical vapor deposition, reactive ion etching, and epitaxial film growth are largely dependent upon the interaction of gaseous species with a semiconductor surface. Often, the technological procedure is a complex mixture of elementary processes at the surface. It is desirable to have chemical and physical methods for studying these elementary processes in detail in order to acquire insight into the factors which control the complex technological procedures, or to enable the invention of new technological methods for semiconductor processing.

This paper describes simple and effective methods for understanding the chemical reactions which occur on semiconductor surfaces. Although many of the semiconductor technological processes are carried out in high pressure or plasma environments, the objective of understanding the elementary surface processes can best be met by studies carried out in ultrahigh vacuum, where control of the surface chemistry may be achieved without interference from the effects of impurities or side reactions.

II. PREPARATION AND MOUNTING OF SEMICONDUCTOR SINGLE CRYSTALS FOR STUDIES IN AN ULTRAHIGH VACUUM ENVIRONMENT.

Semiconductor single crystal wafers are prepared by standard orientation and cutting techniques, followed by polishing and

chemical cleaning in the laboratory atmosphere. The final cleaning is achieved in ultrahigh vacuum using either ion bombardment or chemical procedures.

A simple and highly successful mounting procedure [1] for Si wafers is shown in Figure 1. The rectangular wafer is prepared by sawing 0.25 mm wide slots along three edges of the 1.5 mm thick crystal as shown in the figure. Two of these slots receive ohmic heating contacts made of 0.1 mm Ta sheet bent to fit over 1.0 mm diameter W support rods in a fashion that permits the Ta sheet to form a spring contact inside the Si slot. A third spring contact is welded to a thermocouple junction and spring-loaded into the third slot. The geometrical arrangement shown in Figure 1 is useful in the following ways:

1. All heated metal surfaces are out of line-of-sight contact with the front surface of the Si crystal, preventing high temperature chemistry on the metal from influencing the semiconductor surface.
2. Good ohmic contact is achieved.
3. Good thermocouple contact is achieved as indicated by excellent agreement (± 5K) between pyrometer and thermocouple measurements.
4. Excellent thermal contact between the crystal and the liquid-nitrogen cooled sapphire mounting block is achieved, and crystal temperatures of 90K may be obtained.

A second procedure for mounting semiconductor crystals has been devised as shown in Figure 2. Here, for semiconductor

crystals which are irregular or too hard for convenient sawing, a high temperature cement may be used to mount the crystal onto a W support disk. We have found that the cement Ultratem 516 (Aremco) is particularly convenient for attachment. The insulating adhesive may be mixed with a small amount of graphite to insure sufficient electrical conductivity to avoid charging during studies by XPS or Auger methods. Our measurements indicate that minimal outgassing occurs from this adhesive up to 1400K. Prior to cementing, the W disk may be spot welded to supporting wires of W or Ta which connect to the remainder of the mounting assembly. It is also possible to attach small diameter thermocouples to the crystal using a 90%/10% Au/Ta alloy (mp = 1450 K) which wets the metal and semiconductor surface. Attachment must be done in a preparative vacuum chamber to avoid gross oxidation of the metals. The procedures illustrated in Figure 2 have been employed with SiC crystals [2], but are also applicable to almost any crystal.

III. HEATING AND TEMPERATURE PROGRAMMING OF SEMICONDUCTOR CRYSTALS.

A. Heating Methods

Resistive heating of semiconductors is complicated by the temperature dependent decrease in resistivity of semiconducting materials. This is shown graphically in Figure 3, where a nominally 10 ohm-cm Si crystal of dimensions shown in Figure 1 is subjected to a 16 volt dc bias, using a current limited power

supply. A highly non-linear temperature program results, and the voltage must be reduced as the temperature rises above about 600 K for this particular crystal. In the absence of the current control at the critical temperature, a runaway situation could develop leading to the destruction of the crystal. For this reason, feedback techniques are generally more satisfactory, and high temperature crystal annealing is readily accomplished by means of a thyristor-controlled power supply which is schematically shown in Figure 4. For temperature programming, a well-designed digital programmer that could be modified for use with semiconductors has been described in reference [3].

Another simple technique for temperature programming involves radiative heating techniques [4-6]. A highly reproducible temperature ramp can be generated by directing a focused beam of light on the crystal mounted in a vacuum system as shown in Figure 5. In this apparatus, a blower-cooled 900 watt tungsten-halogen projector lamp is focused on the semiconductor surface by a condenser lens mounted outside the main viewport of the vacuum chamber. The temperature ramp generated by this method, while non-linear, is quite reproducible to about ± 5K over a time period of several weeks, as shown in Figure 6. Temperature programming up to ~ 900K is readily achieved when conduction losses at the crystal are minimized and when a high speed lens system is employed. A high speed lens is necessary because the energy throughput of a lens is proportional to $(a/l)^2$, where a is the lens diameter and l is the focal length. Highest light transmission is obtained by using a large lens. We have achieved

excellent results with a single glass double convex lens (f/1.32) and a magnification of unity. The throughput is improved by use of a parabolic mirror behind the source and an aspherical condenser lens. A correctly designed aspheric lens corrects for spherical aberration and coma and concentrates more energy into the focused spot. For the chamber viewport material, the use of UV grade sapphire offers little advantage over 7056 glass for tungsten lamp sources. The transmission of both materials is nearly 95% in the near infrared where the spectral radiancy is greatest for tungsten.

B. Temperature Measurements

Crystal temperatures are generally measured by means of a thermocouple junction made of small diameter (< 0.1 mm) thermocouple wire. It is easy to spot weld the thermocouple junction onto a small refractory metal tab, and then wedge the tab into a small slot in the crystal as shown in Figure 1. Use of high temperature adhesives for attaching the thermocouple also works adequately. Highest accuracy is obtained by employment of a reference junction at the ice point. A number of thermocouple materials are commonly used. Two favorites are the W - 3% Re vs. W - 25% Re and the W - 5% Re vs. the W - 26% Re thermocouple. Accurate calibration tables exist from liquid nitrogen temperatures [7] to ~ 2500 K [8] for these thermocouples. The W vs. W - 26% Re couple should be avoided at low temperatures (77 K - 300 K) because it is double-valued in this region. Use of a

single wavelength optical pyrometer to measure semiconductor temperatures must be carried out with extreme caution. Spectral emissivities for many semiconductors are not well characterized, and the effect of dopant levels on brightness has not been adequately addressed in the literature. For silicon, emissivities obtained from the often-quoted 1957 work of Allen [9] result in pyrometer readings 40-50 degrees higher than an ice-referenced thermocouple in the range 1000-1300 K. In contrast, temperatures measured for SiC by the two methods give excellent agreement. Spectral emissivities for many materials are updated regularly by CINDAS, the Center for Information and Numerical Data Analysis and Synthesis at Purdue University. Other common sources are given in references [10,11]. The conversion from pyrometer temperature to true temperature is given in [12]. (**Warning:** It is easy to confuse true temperature and pyrometer temperature in tabulations of spectral emissivity.). The most precise work is guaranteed by referencing the pyrometer to an accurate thermocouple. A simple window correction can be made by comparing the brightness of a radiative source directly and after transmission through the vacuum viewport. This is conveniently carried out by temporarily inserting an extra viewport window in front of the viewport through which the pyrometer measurements are being made.

IV. GAS ADSORPTION ON SEMICONDUCTOR SINGLE CRYSTAL SURFACES.

Often it is necessary to adsorb gases in a controlled manner onto a semiconductor surface using rather high exposures due to

the low sticking coefficients involved. The use of a method in which the entire ultrahigh vacuum system is backfilled with the gas to high pressure is unacceptable due to wall effects in which the displacement of impurities occurs, or to interactions with the thermionic emitters in ionization gauges or mass spectrometers, or to regurgitation effects in the ion pumps which will cause contamination of the gas phase.

The use of a molecular beam doser alleviates these effects and permits the use of relatively high adsorption fluxes without the production of high gas loads within the ultrahigh vacuum system. These sources may involve the use of a microchannel plate collimator to achieve uniformity of flux across the crystal surface [13] or may instead involve just the use of a tubular effusion source.

A diagram of the basic design for the molecular beam doser is shown in Figure 7. Here in the expanded portion of the figure a simple design for holding the microcapillary channelplate collimator is shown. A baffle inside the cylindrical support assembly insures that beaming into the backside of the capillary array does nor occur. The control of the effusion rate is achieved by using a ~ 2 micron diameter orifice (obtainable from the Buckbee Mears Co.) which is compression-mounted inside a VCR fitting between two Cu or Ni gaskets. In constructing this assembly it has been found helpful to rivet the two gaskets and the orifice with three thin Cu wires to prevent rotation of the gaskets against the orifice during compression [14]. Leak-tight assemblies are easily made with practice.

The control of gas flow through the orifice and the collimator is achieved by the use of a gas-handling line schematically shown in the bottom of Figure 7. Here, using Baratron capacitance manometers and separate pumping, the gas flow through the orifice may be adjusted quantitatively. This arrangement is of value in providing a controlled flux of gas to the single crystal under conditions where high purity is maintained, since gases are handled at relatively high pressure up to the orifice inside the UHV system, and dilution with background gases is minimized. In addition, by controlling the flow at a point close to the doser outlet inside the vacuum system, rapid response is achieved. A measurement of the response of the mass spectrometer to a controlled pulse of propylene through the molecular beam doser system is shown in Figure 8. An approximate square pulse shape is detected. Behavior at the crystal face is probably more ideal than the mass spectrometer signal shown here.

The angular distribution of gas emitted from this orifice has been throughly investigated, and details are given in [15]. Calibration of the effusion source is accomplished using standard volumetric methods. A typical value for the total flux of gas from such a source is $\sim 10^{14}$ molecules/torr-sec. This technique enables determination of the absolute surface coverage and sticking probability [16].

In summary, the use of the molecular beam doser for adsorption of gases onto a semiconductor surface offers the following advantages:

1. Reduction of vacuum system gas load.
2. Precise and accurate fluence onto the crystal.
3. Reduction of impurity levels in the incident gas.
4. Prevention of intermolecular collisions in the incident gas, allowing no possibility of gas excitation by interaction with species which may desorb from a heated surface being dosed [1].

V. REACTIVE CHEMISTRY AT SEMICONDUCTOR SURFACES.

Several fundamental studies of semiconductor surface chemistry are possible by using the methods described above. Studies of adsorption phenomena, chemical bonding, surface composition, adsorption kinetics, surface reactivity, and diffusion are readily performed. By using thermal desorption as a probe of surface reactivity [16], a vast range of surface chemistry can be investigated. These measurement techniques can be used to observe the creation and destruction of active surface sites. Several examples from our recent work on silicon and silicon carbide illustrate some of the possibilities. The methods described should be generally useful in studies of semiconductor surface chemistry.

A. Investigation of Bonding Sites on Semiconductor Surfaces.

Thermal desorption techniques may be used to provide information on the energetics of bonding, the chemical nature of bound species, and the reactivity of adsorbed molecules with semiconductor surfaces. For example, population of the active sites

available to propylene during interaction with Si(100) - (2 x 1) are shown in Figure 9. The silicon surface was prepared by 2 kV Ar^+ sputtering, followed by high temperature annealing in vacuum at 1100 K to produce a well-ordered surface.

For the case of C_3H_6 on Si(100), two desorption states are observed. One is a weaker binding state of high population which desorbs at about 550 K, while the other is a stronger binding state of low relative population desorbing at 590 K. The controlled doses of propylene were applied at a crystal temperature of 130 K with the molecular beam technique described above. Following the analysis of Chan and coworkers [17] for first-order kinetics, the desorption energy was estimated to be 1.2 ev and the preexponential factor was 9.3×10^9 s^{-1}. That the desorption peak shifts to higher temperatures as the C_3H_6 coverage increases is indicative of lateral attractive interactions between the adsorbed species. Other intact hydrocarbon molecules stable at high temperatures have also been observed on silicon [18].

B. Determination of Branching Ratios in Surface Decomposition of Adsorbed Molecules.

The reaction pathways available to an incident molecule and the extent of surface reactivity may be easily measured by Auger analysis before and after thermal desorption. An example for propylene interaction with Si(100) is provided in Figure 10. By plotting the C/Si Auger peak ratio vs. C_3H_6 exposure before and after C_3H_6 desorption, it is observed that only ~ 40% of the

adsorbed propylene bonds intact. The remainder of the adsorbed C_3H_6 dissociates to form a carbon-containing overlayer. There are thus at least two reaction pathways for C_3H_6 on Si(100). For a complete analysis, it is necessary to examine other molecular species likely to desorb as a result of fragmentation on the surfaces. This is most readily accomplished with a multiplexed mass spectrometer which can monitor several desorbing species simultaneously. Our studies of C_3H_6 on Si(100) have shown that only propylene desorbs at temperatures below 1000 K, suggesting that hydrogen fragments from C_3H_6 are incorporated into the Si crystal, and that once C-H or C-C bond breaking occurs, non-volatile surface species are produced.

C. Kinetic Observation of Molecular Adsorption.

The kinetics of the reaction between an incident gas molecule and a semiconductor surface may be examined by rotating the crystal into a beam of the adsorbing species while monitoring the scattered signal with a mass spectrometer. An interesting comparison is possible when the experiment is carried out in two ways: (1) adsorption on an ordered, annealed semiconductor surface; (2) adsorption on a disordered, ion-bombarded semiconductor surface. We show below that surface reactivity is considerably different for these two cases.

The kinetics of adsorption for a molecular beam of C_3H_6 on Si(100) is shown in Figure 11, for studies done in the UHV system shown in Figure 5. The solid curve represents the reaction of propylene with an ordered Si(100) surface, and the dashed curve

represents the reaction of propylene with a disordered Si(100) surface. The propylene flux to the crystal was the same in both cases (5.9×10^{12} molecules/cm^2 sec). During interception of the beam by the surface, the partial pressure of the unreacted propylene scattered from the crystal rapidly decreases to a constant value as uptake by the crystal occurs. For the case of C_3H_6 on Si(100), the constant value is indicative of a coverage-independent sticking probability. The sticking probability remains constant until the crystal is saturated, and then the flux of scattered C_3H_6 begins to rise as the reflection of the propylene increases. Beyond the end of the adsorption region, the abrupt rise in the scattered propylene pressure signals a decrease in the adsorption rate on Si(100).

It is observed that a disordered Si(100) surface is saturated faster with C_3H_6 than an ordered Si(100) surface. Since the total flux of propylene was the same for each case, it is likely that the bombarded surface produces higher coverages of fragments of several types from dissociation of C_3H_6, which reduces the capacity of the disordered surface to adsorb propylene. We show below that ion bombardment induces dissociation chemistry by the production of active sites on the semiconductor surface.

D. Thermal Desorption Studies of the Production of Reactive Sites by Ion Irradiation.

The adsorption of molecular species on semiconductor surfaces depends strongly on the availability of active sites at the surface. As shown in Figure 11, reactive sites can be produced

by Ar^+ ion bombardment. The increase in reactivity is due to an increase in dissociative chemisorption which occurs at defect sites produced by the ion beam. By performing the irradiation before the adsorption, it is possible to vary the surface reactivity in a controlled way without the complications of other processes such as ion-induced dissociation of adsorbed layers and free radical production in the gas phase. Previous studies have focused on the effect of ion irradiation during adsorption, and are likely to include ion-induced dissociation of adsorbates as well as surface defect formation [19-20].

In a typical experiment, the semiconductor surface is prebombarded with a defocused beam of Ar^+ ions. A controlled dose of adsorbed molecules is added to the damaged surface. Temperature programmed desorption is then carried out in the usual fashion. The results for C_3H_6 on Si(100) are shown in Figure 12. The crystal was prebombarded with varying ion fluences before adsorption of a constant dose of propylene. The desorption curves show that increasing surface disorder by ion bombardment results in greater chemical reactivity. This is seen by the reduction in propylene desorption yield with ion fluence [21]. The fact that such small ion currents (~ nanoamps) affect the surface chemistry has fundamental implications for several semiconductor technologies.

E. Suppression of Reactive Sites by Hydrogen Adsorption.

Just as semiconductor surface reactivity may be increased by production of surface defects, it may be decreased by surface

capping of active sites by preadsorbed molecules. For example, preadsorbed atomic hydrogen acts to prevent propylene adsorption by occupation of active surface sites. This is demonstrated in Figure 13. Varying doses of atomic hydrogen were adsorbed onto a clean, annealed Si(100) face and then a constant dose of C_3H_6 was added. The hydrogen was easily produced by molecular dissociation of $H_2(g)$ to 2H(g) at a hot (≈ 2100 K) tungsten filament in the vacuum chamber which was located in a line of sight geometry to the Si(100) crystal. The resulting desorption curves show that lower hydrogen preexposures are accompanied by higher propylene desorption yields. The reduction in desorption yield caused by H-surface capping is due to a reduction in propylene adsorption capacity on the hydrogen-covered surface rather than an increase in molecular dissociation at the surface. In other words, fewer molecules of propylene have desorbed because fewer have adsorbed on the surface exposed to H atoms. This has been shown by kinetic studies of C_3H_6 adsorption on the H-covered surface using methods described in detail above [21,22].

F. Manipulation of Reactive Surface Chemistry.

For Si(100), a full range of reactive chemistry may be produced by the combined operation of active site production and active site destruction. This allows considerable latitude in the ability to manipulate silicon surface chemistry and has fundamental implications for processes of chemical vapor deposition and reactive ion etching. We illustrate the range of chemistry by reference to Figure 14.

In this figure, the combined influence of ion prebombardment and hydrogen preadsorption is shown by adsorption-kinetic observation of propylene adsorption. The results on an ordered, annealed surface are compared to an ion-bombarded, disordered surface. It is observed that simple kinetic techniques provide considerable information about the reaction of adsorbed gases with a semiconductor surface. The adsorption-kinetic methods can be especially important in studies of extremely reactive systems where most of the adsorbate reacts and no desorption products are observed. Three classes of reflected signal are present in Figure 14 which depend on the availability of active sites on the surface. In the first class (denoted by I), propylene reacts with clean, ordered Si(100) with a constant sticking coefficient. In the second class (denoted by II), propylene reacts with prebombarded, disordered Si(100) to produce a reflected signal which saturates faster than ordered Si(100). In the third class (denoted by III), propylene reacts with a Si(100) surface containing a preadsorbed overlayer of hydrogen produced by atomic H irradiation. For both ion-bombarded and annealed cases, the reflected signal indicates faster termination of propylene uptake with higher hydrogen coverages. This shows that the two effects (site production and site destruction) may be played against one another, and that the sites produced by ion bombardment can be subsequently capped by hydrogen adsorption.

VI. CONCLUSIONS

This paper has presented a description of several experimental methods which are useful in the investigation of the elementary steps which occur at semiconductor surfaces undergoing chemical reaction with gaseous species. By working at low adsorption temperatures in an ultrahigh vacuum environment it is possible to separate elementary steps and to study the individual steps in some detail. This simplification is generally not possible in investigations of CVD processes at high pressure or of PVD processes in a plasma since a combination of elementary chemical and physical steps exist under normal CVD and PVD conditions. The methods described in this paper are mainly derived from principles developed to study chemistry at metal surfaces [16], and involve the use of a simple ultrahigh vacuum apparatus.

VII. Acknowledgments

We gratefully acknowledge support of this work by AFOSR under Contract No. F49260-84-C-0063DEF. We also acknowledge helpful discussions with Dr. William Partlow of the Westinghouse Research Laboratory, Pittsburgh, Pennsylvania.

REFERENCES

1. F. Bozso, J. T. Yates, Jr., W. J. Choyke, and L. Muehlhoff, J. Appl. Phys., 57, 2771 (1985).
2. F. Bozso, L. Muehlhoff, M. Trenary, W. J. Choyke, and J. T. Yates, Jr., J. Vac. Sci. Technol., A2(3) 1271 (1984).
3. R. J. Muha, S. M. Gates, J. T. Yates, Jr., and P. Basu, Rev. Sci. Instrum., 56(4), 613 (1985).
4. R. E. Weber and W. T. Peria, J. Appl. Phys., 38, 4355 (1967).
5. T. E. Madey and J. T. Yates, Jr., Structure et Proprietes des Surfaces des Solides, No. 187, pp. 155-162 (Centre National de la Recherche Scientifique, Paris, France, 1970).
6. J. T. Yates, Jr. and D. A. King, "Chemisorption of CO on Tungsten (100): Combined Flash Desorption and Electron Stimulated Desorption Study. I.", Surface Science 32, 479-505 (1972).
7. D. R. Sandstrom and S. P. Withrow, J. Vac. Sci. Technol. 14, 748 (1977).
8. ASTM Publication E988.
9. F. G. Allen, J. Appl. Phys. 28, 1510 (1957).
10. D. N. Baria and R. G. Bautista, Compilation of Experimental Work on Thermal Emittances of Materials Part II--Nonmetals, Ames Laboratory, USAEC, Iowa State University, April 1974. Available from the National Technical Informaion Service, Springfield VA 22151.
11. Y. S. Touloukian and D. P. DeWitt, Thermal Radiative Properties--Nonmetallic Solids, Vol. 8, Plenum, New York, 1972.

12. D. E. Poland, J. W. Green, and J. L. Margrave, NBS Monograph 30, April, 1961.

13. For one example from our laboratory, see J. N. Russell, S. M. Gates, and J. T. Yates, Jr., "Reaction of Methanol with Cu(111) and Cu(111) + O(ads)", Surf. Sci. 163, 516 (1985).

14. We thank Professor John Hemminger, University of California - Irvine, for this helpful suggestion.

15. C. T. Campbell and S. M. Valone, J. Vac. Sci. Technol. A 3(2), 408 (1985).

16. J. T. Yates, Jr., in Methods of Experimental Physics, Vol. 22, pg. 425-464, Academic Press, 1985.

17. C. M. Chan, R. Aris, and W. H. Weinberg, Appl. Surf. Sci. 1, 360 (1978).

18. P. Klimesch, G. Meyer, and M. Henzler, Surf. Sci. 137, 79 (1984).

19. J. W. Coburn and H. F. Winters, J. Vac. Sci. Technol. 16(2), 391 (1979).

20. J. W. Coburn and H. F. Winters, J. Appl. Phys. 50(5), 3189 (1979).

21. M. J. Bozack, W. J. Choyke, L. Muehlhoff, and J. T. Yates, Jr., submitted.

22. M. J. Bozack, W. J. Choyke, L. Muehlhoff, and J. T. Yates, Jr., submitted.

FIGURE CAPTIONS

Fig. 1 Mounting scheme for regularly-shaped semiconductor single crystals.

Fig. 2 Mounting scheme for irregularly-shaped semiconductor single crystals.

Fig. 3 The behavior of current, resistance, and voltage when silicon is resistively heated with a current-limited D. C. power supply.

Fig. 4 Block diagram of the thyristor power supply for resistive heating of semiconductor samples. The circuit consists of a high voltage low current source and a low voltage high current phase regulated unit. Initially the sample is connected to the high voltage source. A sensing amplifier measures the voltage drop across a series resistor which is proportional to the current through the sample. At a particular level, a relay switches the heating circuit to the low voltage, high current power supply. The average current through the sample is then set by the phase angle of the thyristor trigger pulses which in turn is set by the feedback circuitry.

Fig. 5 Ultrahigh vacuum apparatus used to study semiconductor surface chemistry.

Fig. 6 The temperature ramp generated by a 900 W tungsten-halogen radiative light source focused on the silicon crystal. The reproducibility is about ± 5K over several weeks.

Fig. 7 Molecular beam doser and associated gas handling system for accurate adsorption measurements. The collimated beam is produced using a microcapillary array containing 10μ capillaries of length 500μ. Effusion rates are controlled by the 2μ orifice which is sandwiched between Cajon gaskets. Control of gas flow is achieved by manipulation of gas pressure behind the orifice using the valving arrangement shown. The conductance of the orifice is measured by long time pumping experiments which monitor the drop in backing pressure in a known volume section of the gas handling system. It has been found convenient to insulate the capacitance manometers from air currents to achieve the highest stability.

Fig. 8 The on/off characteristics of the molecular beam effusion source, as measured with a mass spectrometer.

Fig. 9 Thermal desorption spectra of C_3H_6 on annealed, ordered Si(100). A bonding site with an activation energy for C_3H_6 desorption of ~ 1.2 eV is indicated.

Fig. 10 The C(272 eV)/Si(92 eV) Auger ratio before and after thermal desorption. About 40% of the propylene bonds intact; the rest dissociates to form a carbon-containing overlayer on silicon, which yields the lower curve.

Fig. 11 Kinetics of C_3H_6 adsorption on ordered and ion-bombarded Si(100). The disordered surface saturates faster.

Fig. 12 The decrease in C_3H_6 thermal desorption yield with increasing fluences of prebombarding Ar^+ ions. The undissociated C_3H_6 yield decreases because more propylene is reacting with the sites created by ion bombardment.

Fig. 13 The effect of preadsorbed atomic hydrogen on clean Si(100). The decrease in the C_3H_6 thermal desorption yield is caused because fewer molecules of propylene adsorb on the surface.

Fig. 14 The dynamics of C_3H_6 adsorption on ordered and disordered Si(100). In Curve I, propylene reacts with annealed, ordered Si(100). In Curve II, propylene reacts with ion-bombarded, disordered Si(100). In Curve III, propylene reacts with an atomic hydrogen-exposed layer on Si(100). The disordered surface saturates faster due to higher molecular fragmentation at the disordered surface, which reduces the capacity of the surface to adsorb more propylene. The H-capped surface saturates faster due to the reduction of sites capable of C_3H_6 adsorption.

Mounting Scheme for Si Single Crystal Specimens

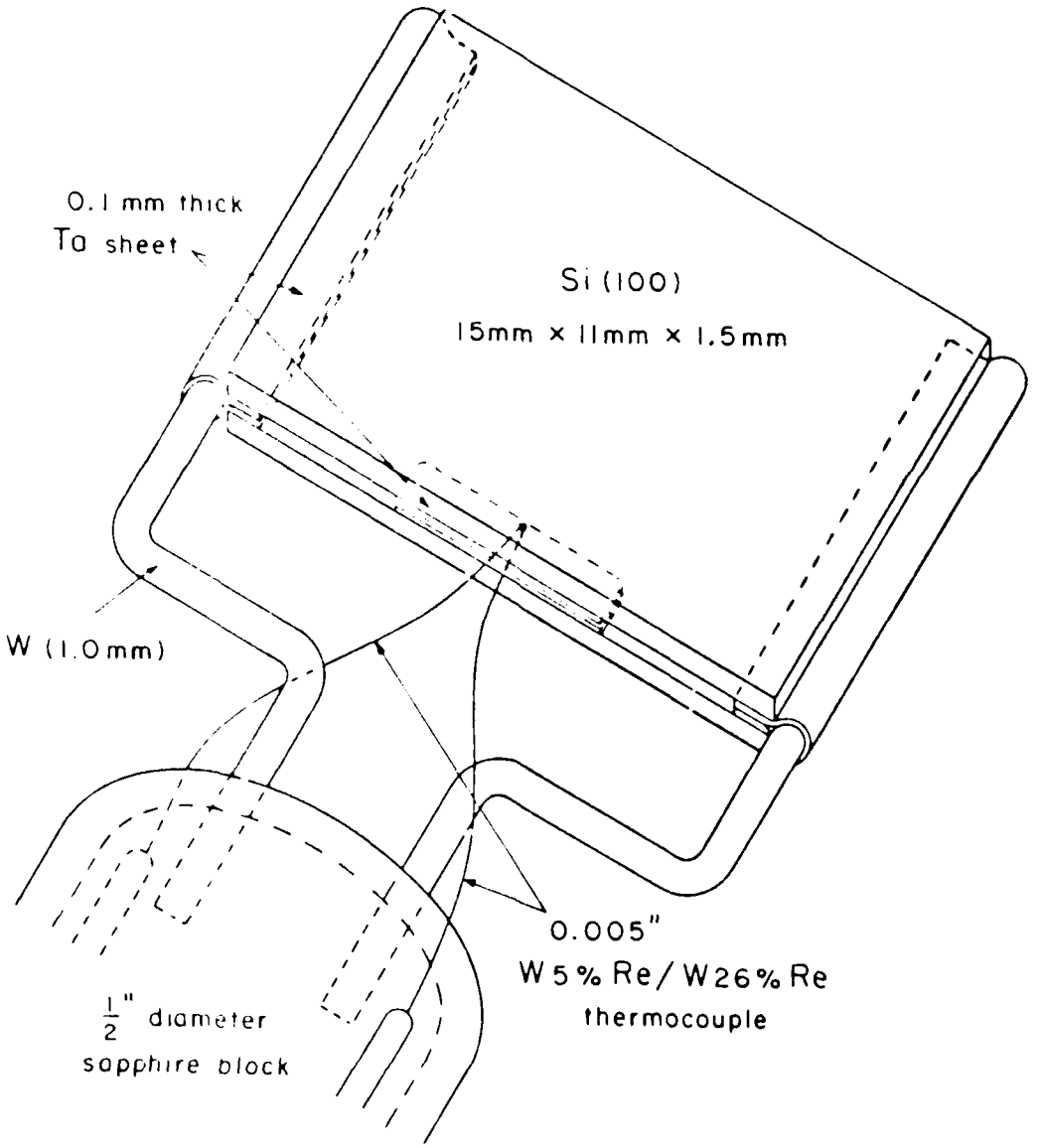

Figure 1.
Bozack
Muehlhoff
Russell
Choyke, Yates

Mounting Scheme for Irregularly-Shaped Semiconductors

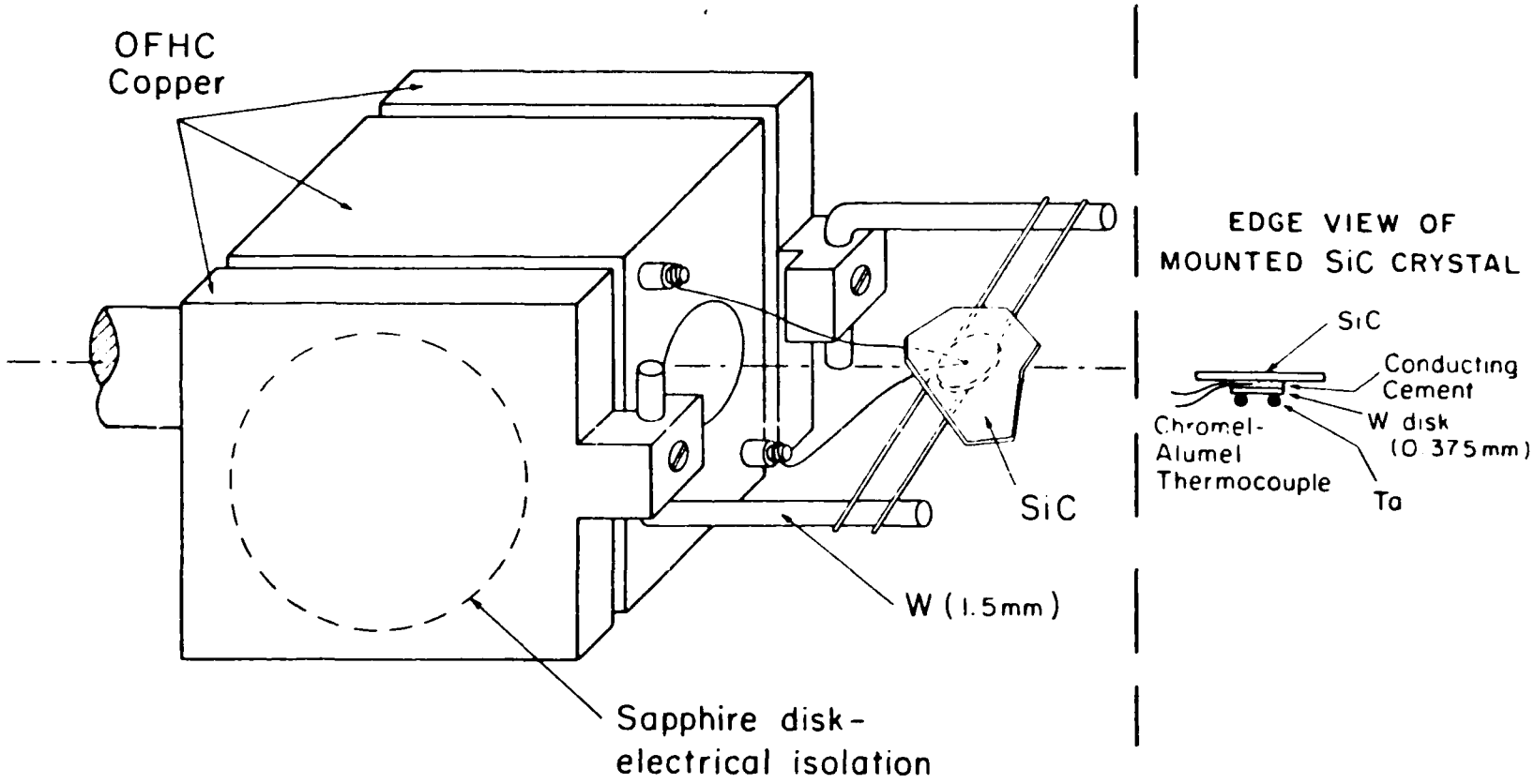

Figure 2.
Bozack
Muehlhoff
Russell
Choyke, Yates

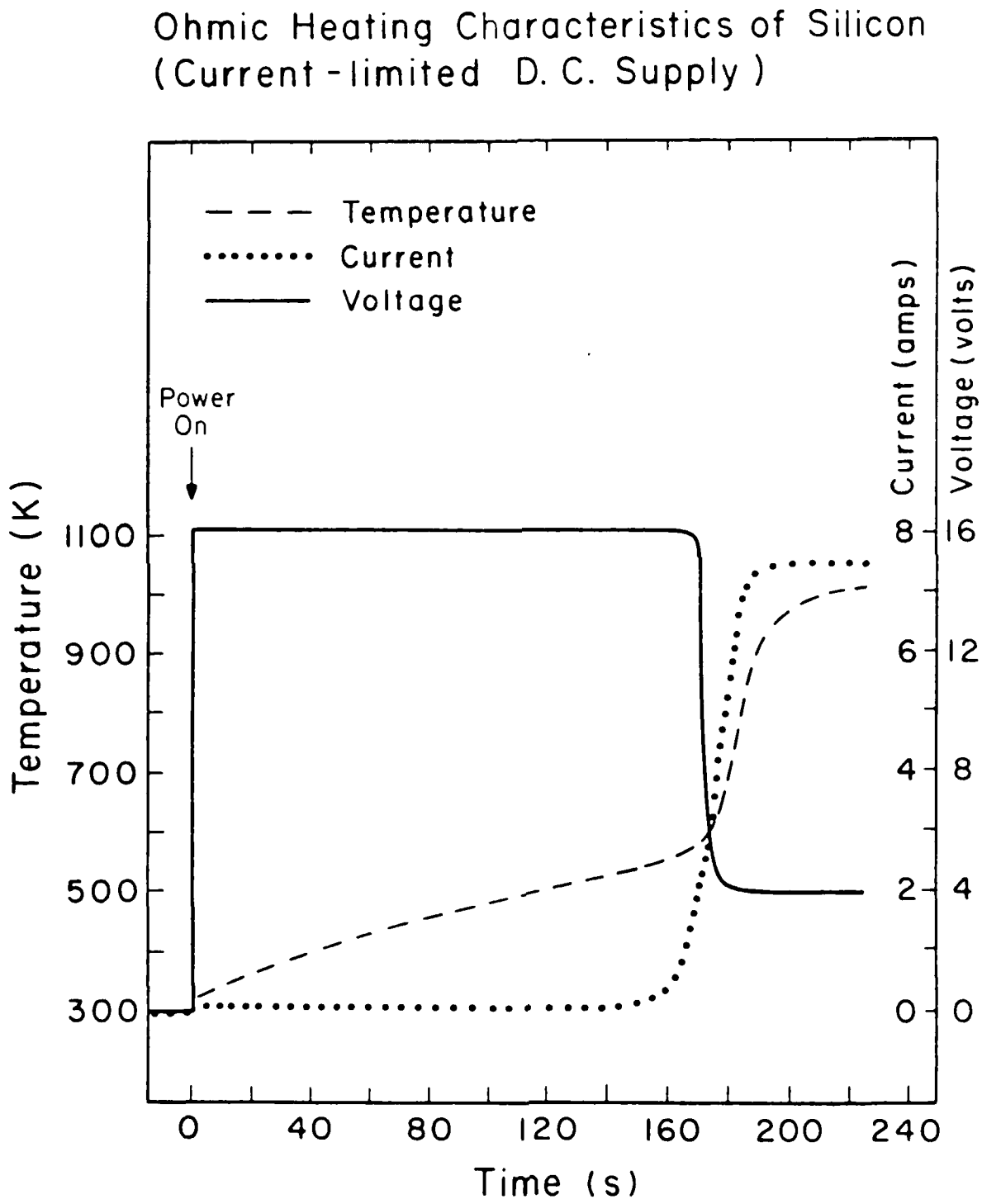

Figure 3.
Bozack
Muehlhoff
Russell
Choyke, Yates

Thyristor Power Supply for the Resistive Heating of Semiconductor Samples

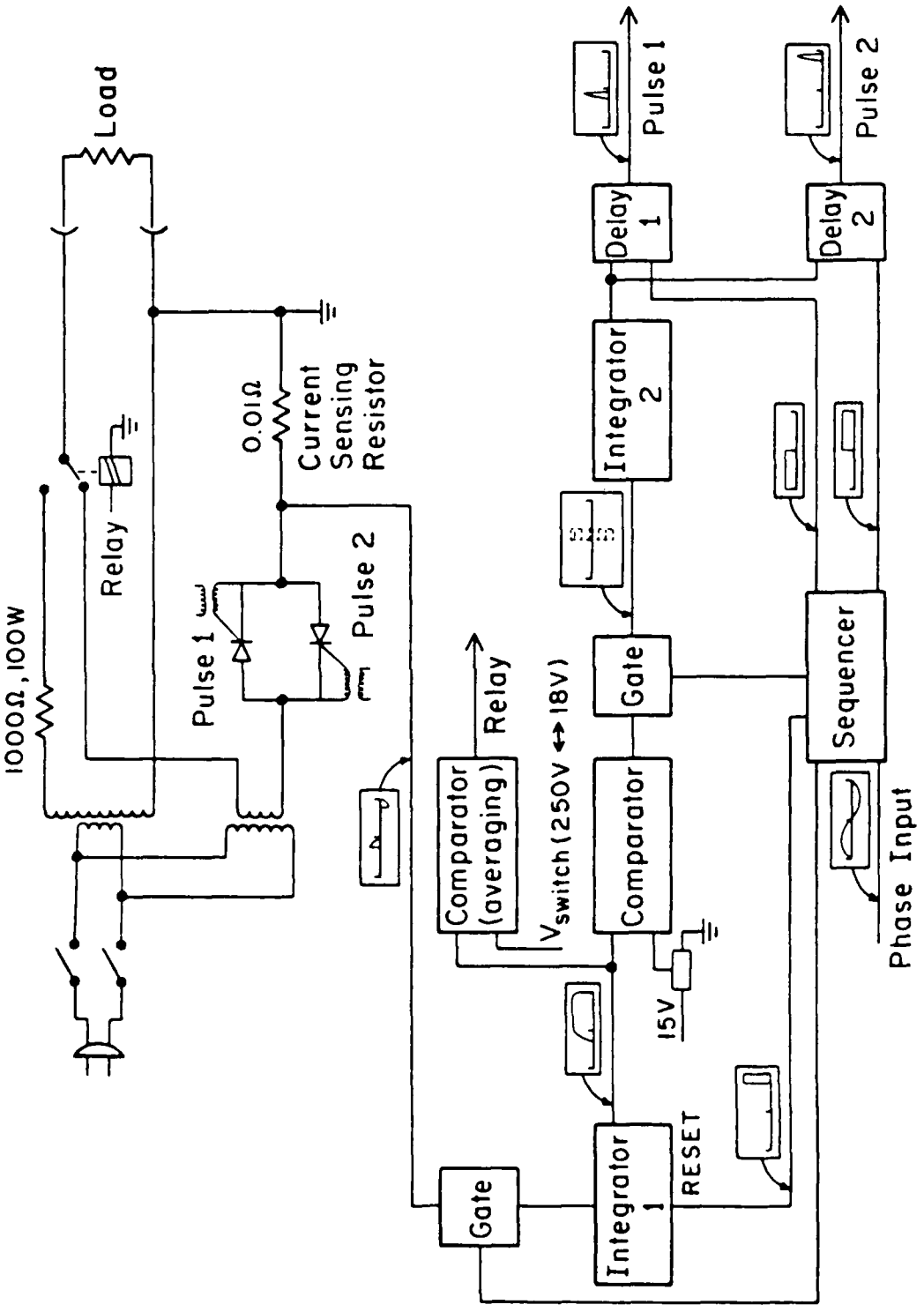

Figure 4.
Bozack
Muehlhoff
Russell
Choyke, Yates

Apparatus Used to Study Semiconductor Surface Chemistry

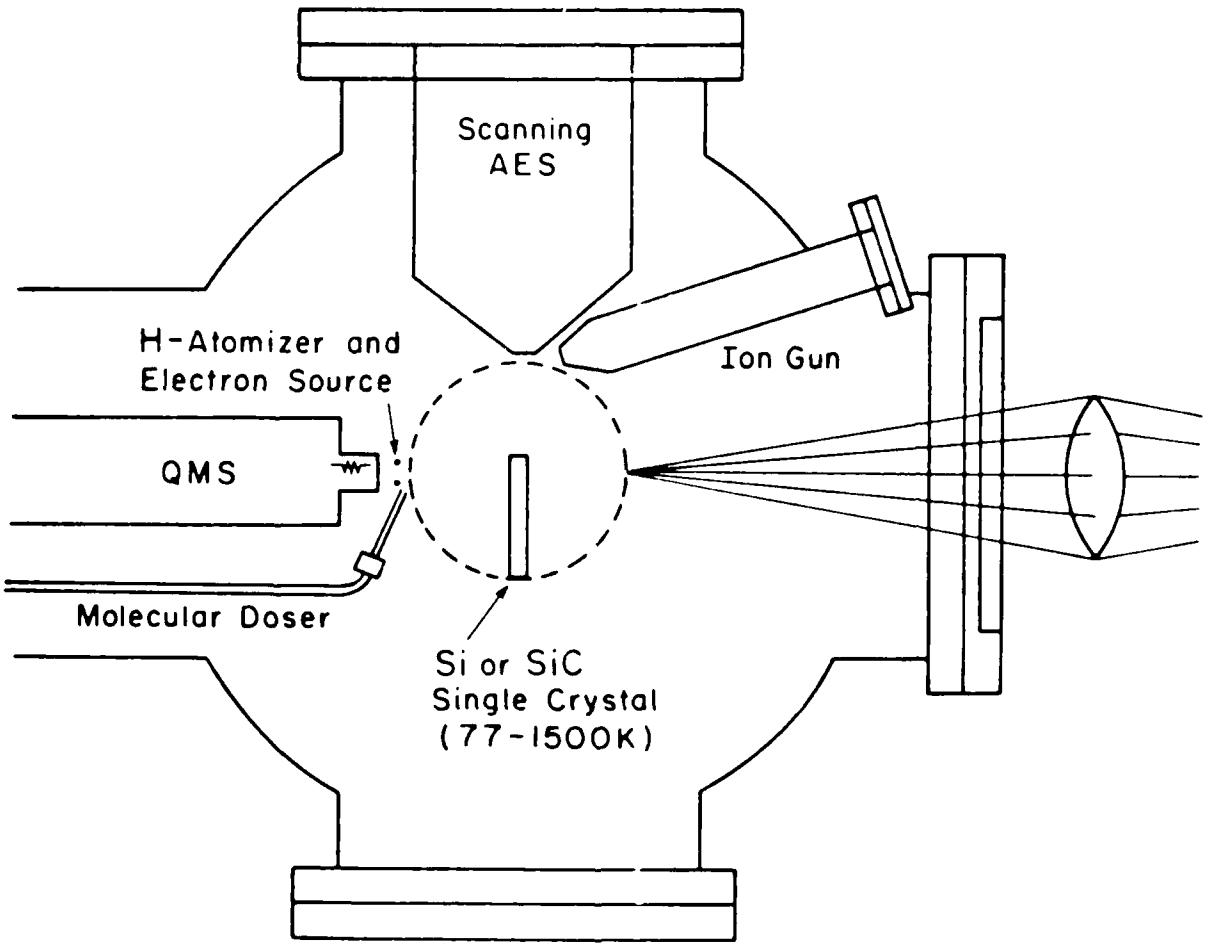

Figure 5.
Bozack
Muehlhoff
Russell
Choyke, Yates

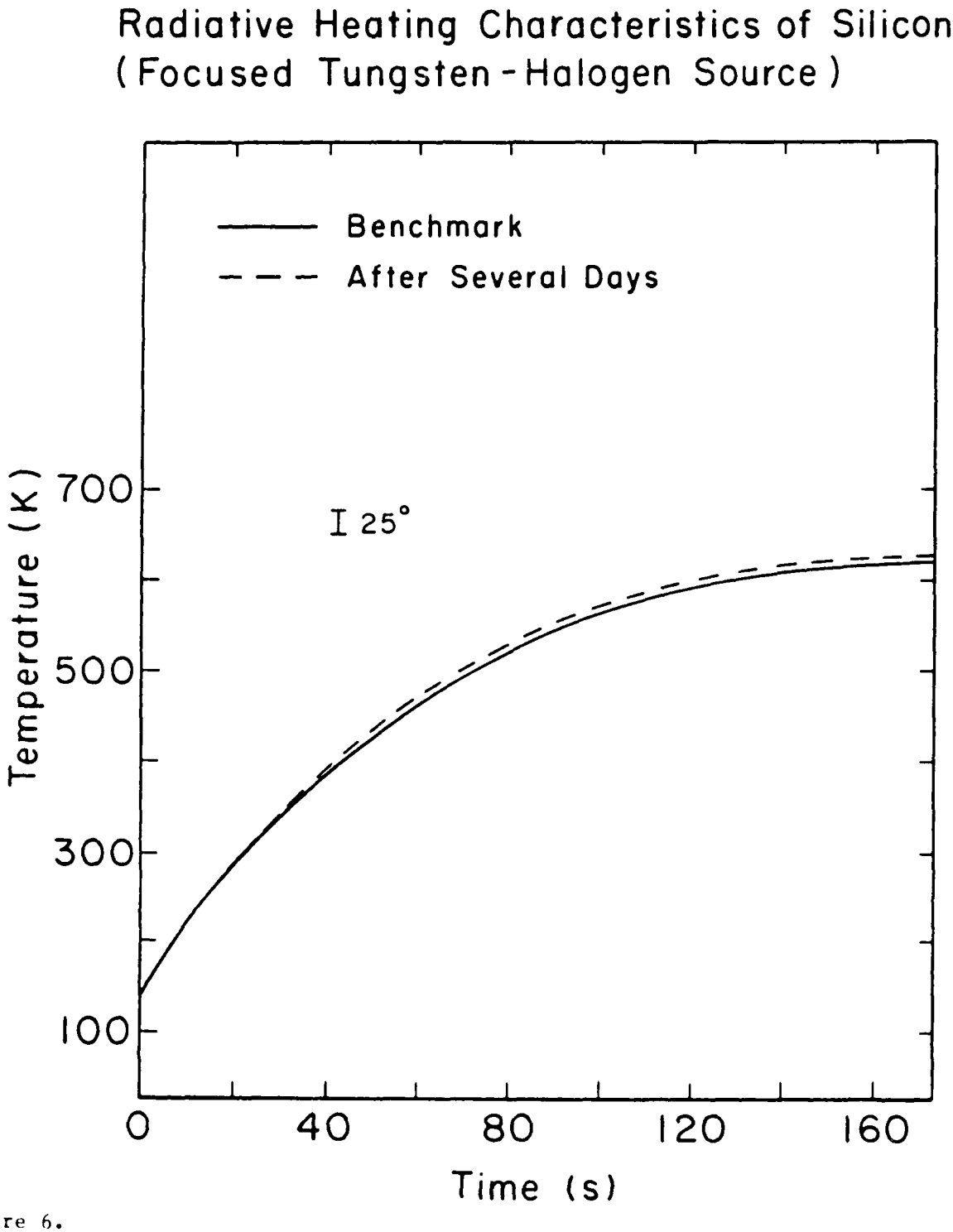

Figure 6.
Bozack
Muehlhoff
Russell
Choyke, Yates

SCHEMATIC DIAGRAM OF MOLECULAR BEAM DOSER – GAS HANDLING SYSTEM

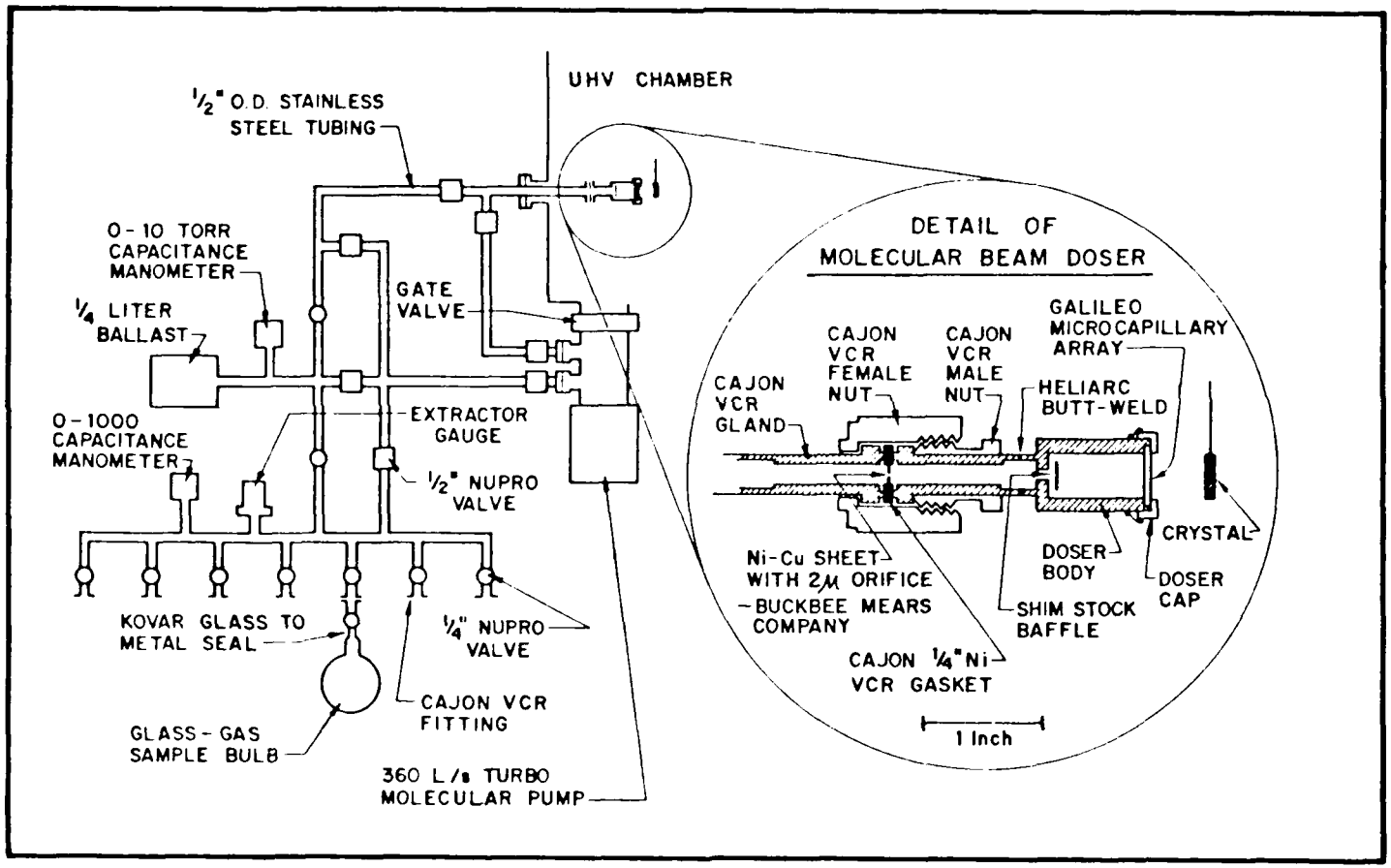

Figure 7.
Bozack
Muehlhoff
Russell
Choyke, Yates

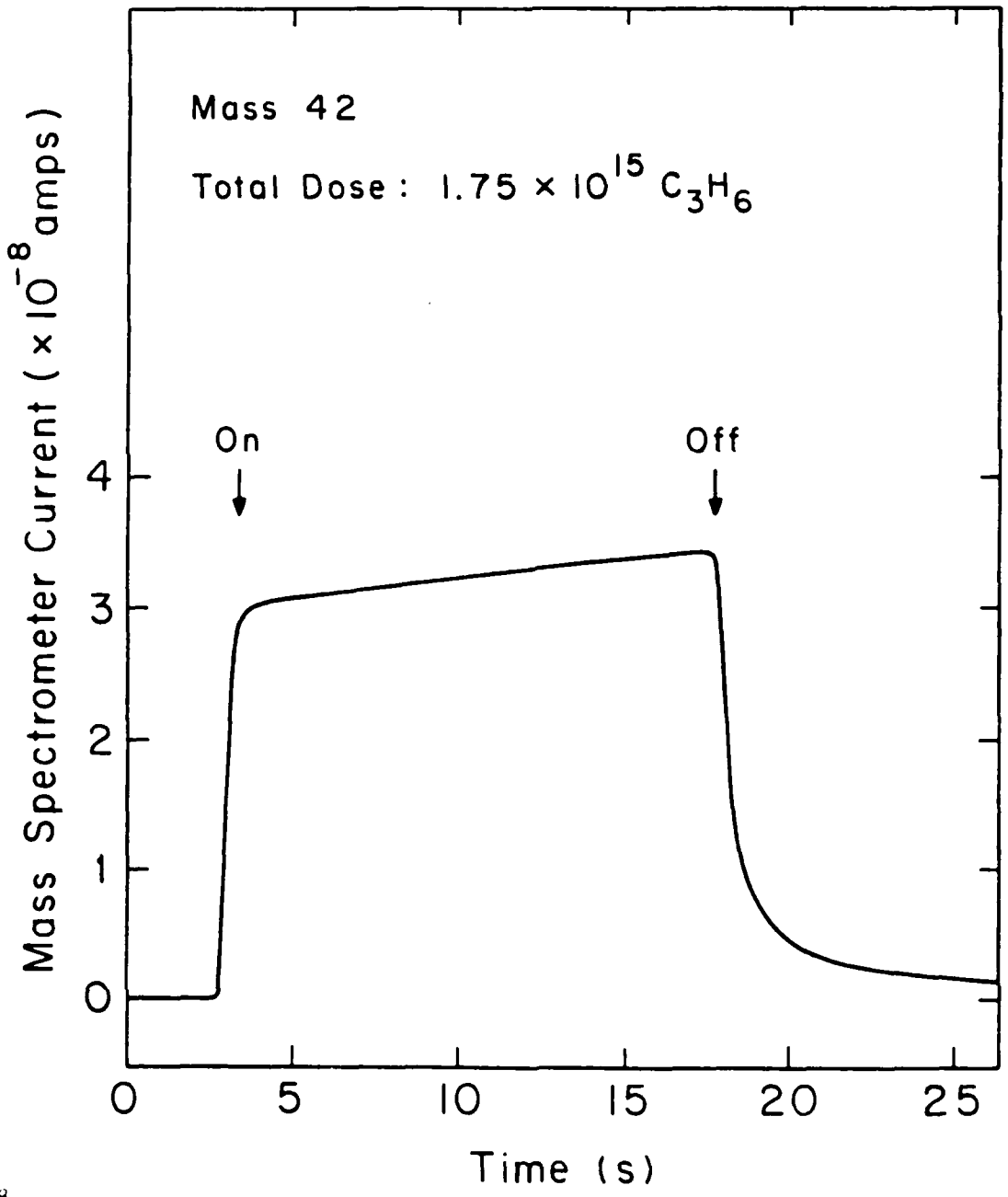

Figure 8.
Bozack
Muehlhoff
Russell
Choyke, Yates

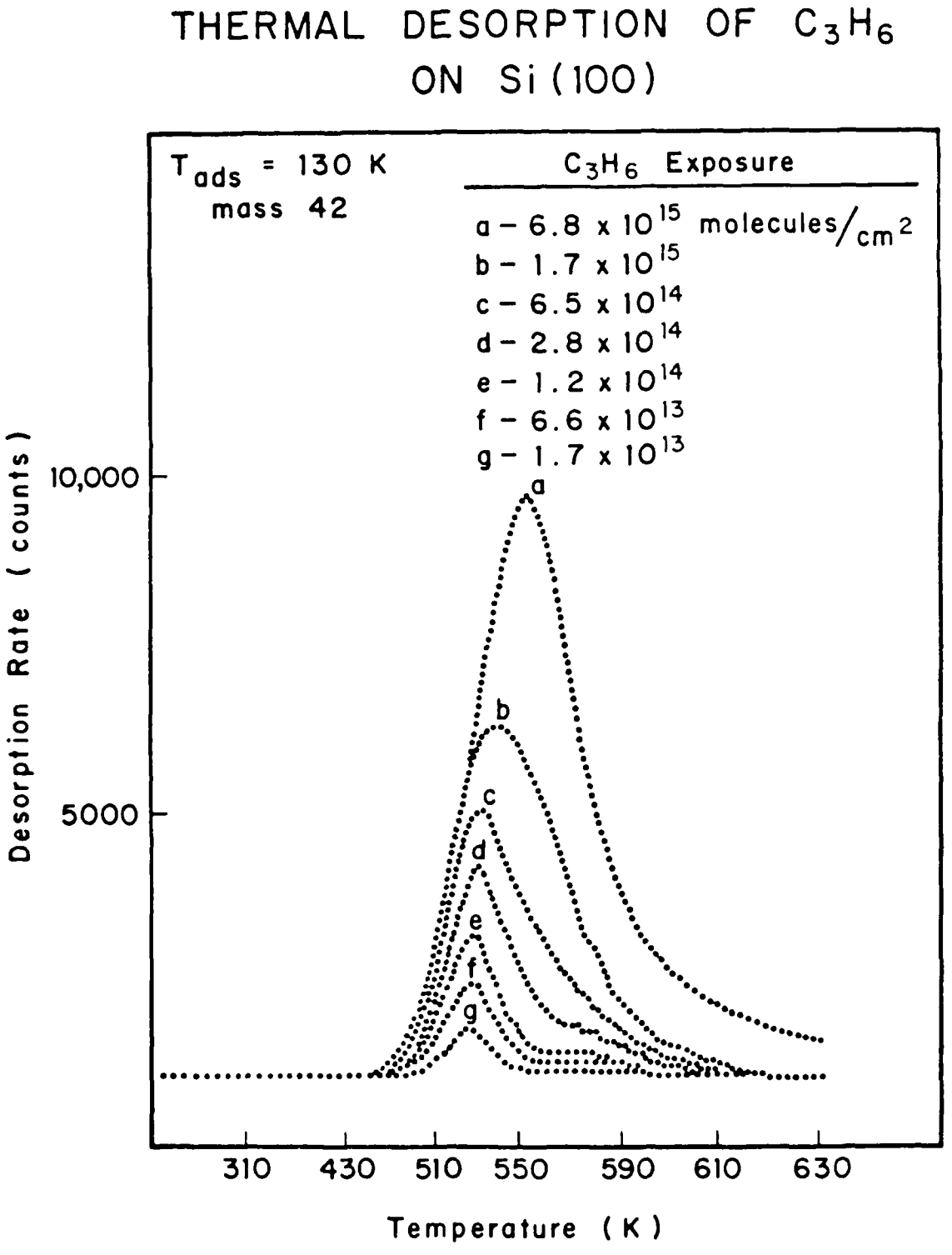

Figure 9.
Bozack
Muehlhoff
Russell
Choyke, Yates

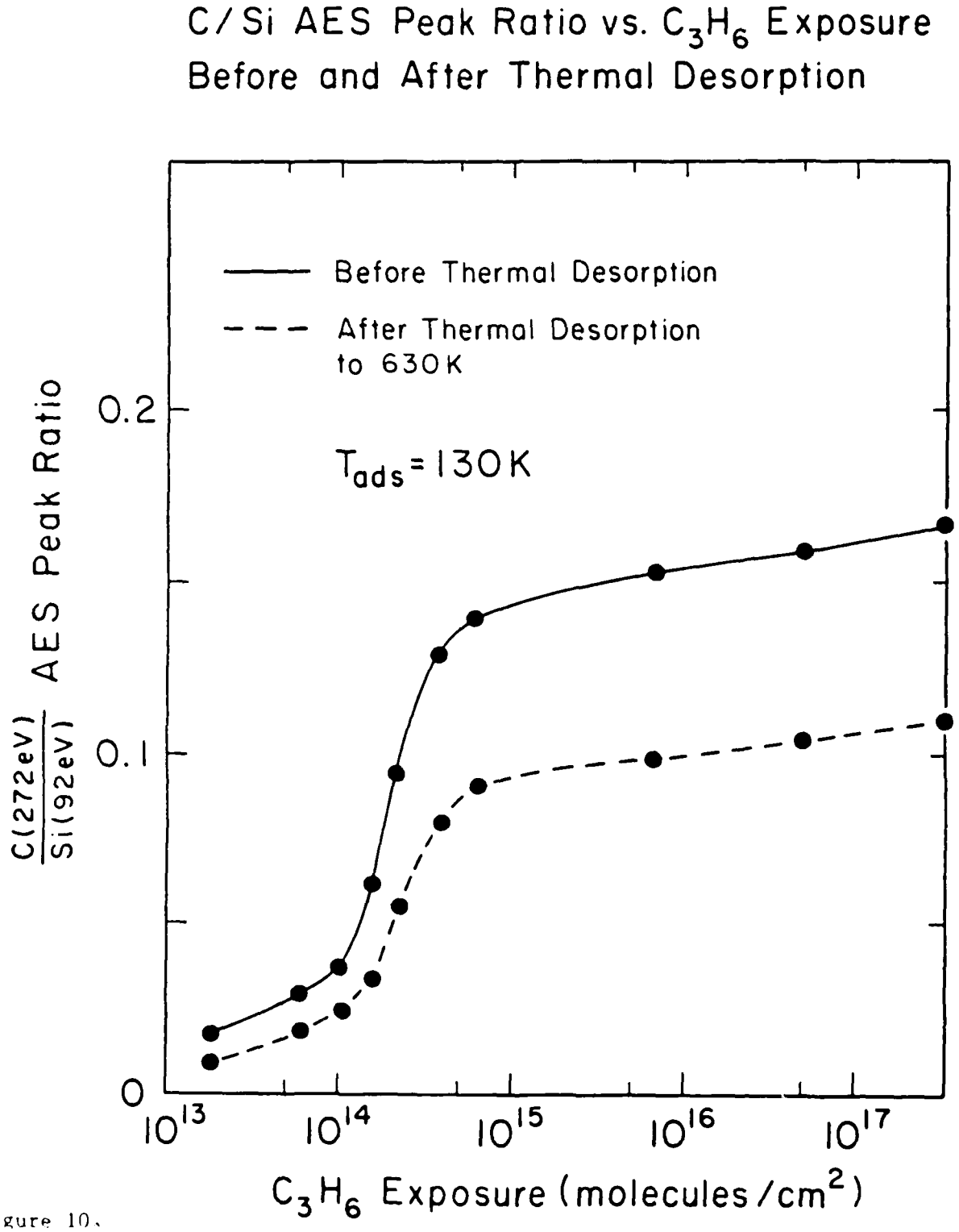

Figure 10.
Bozack
Muehlhoff
Russell
Choyke, Yates

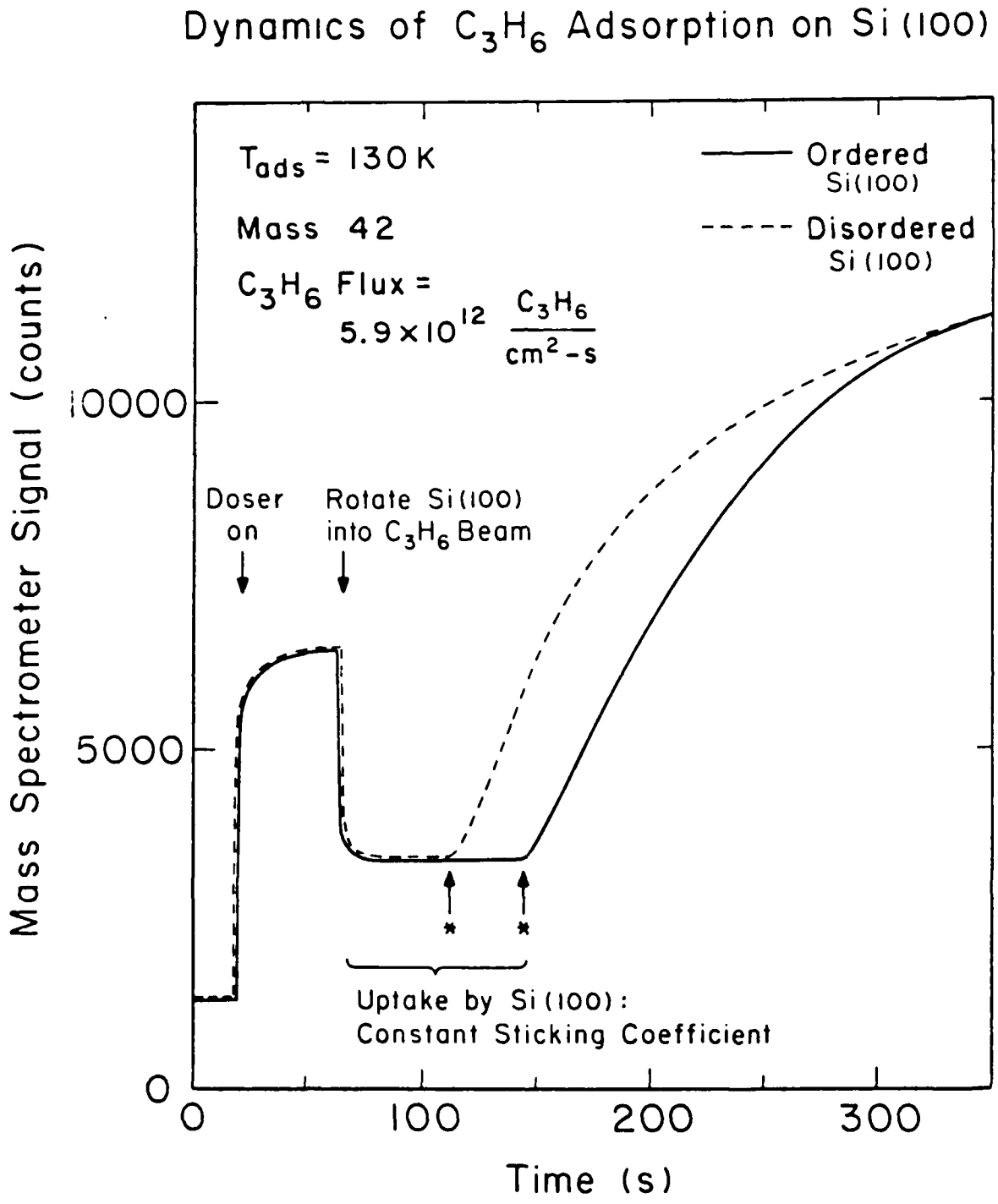

Figure 11.
Bozack
Muehlhoff
Russell
Choyke, Yates

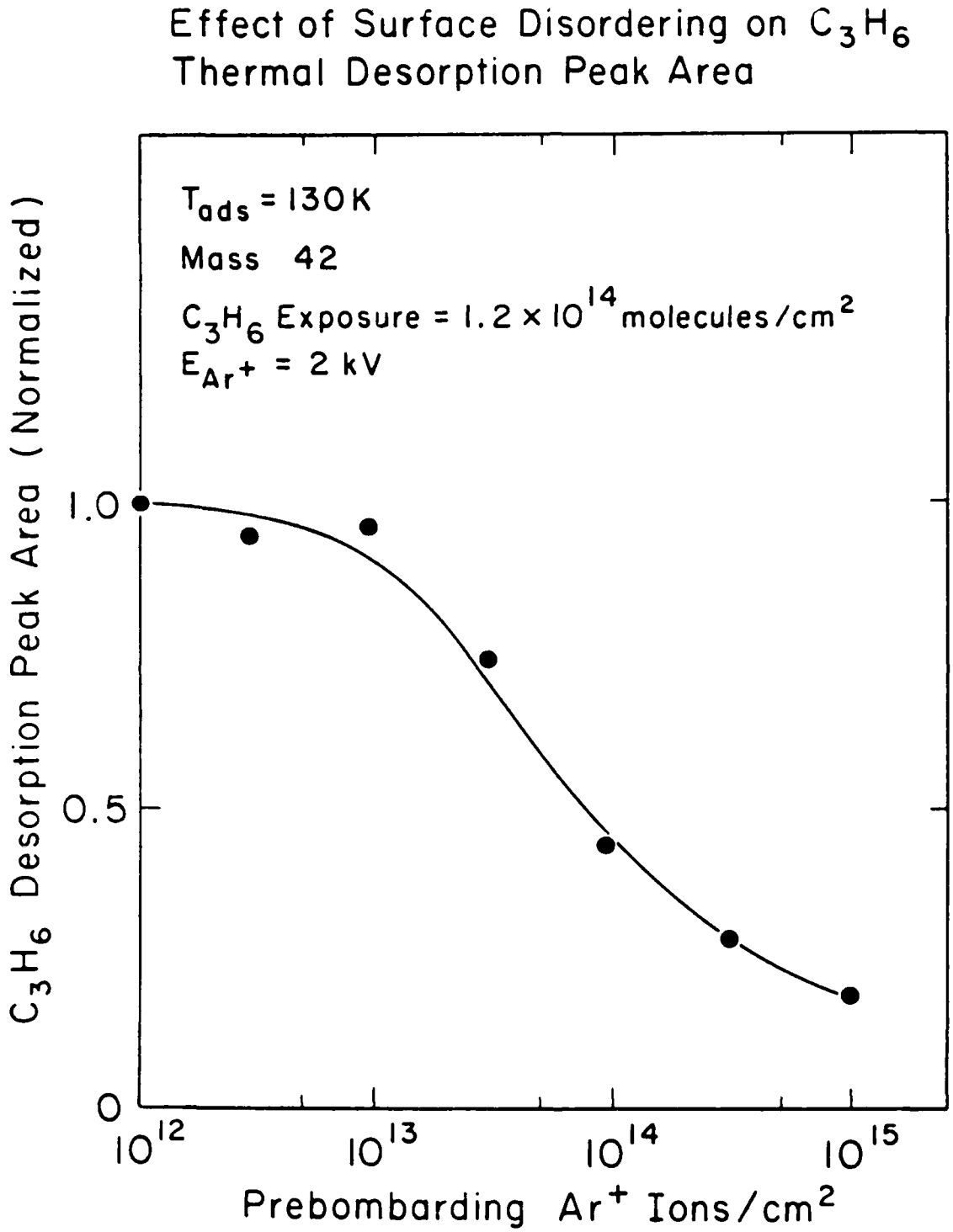

Figure 12.
Bozack
Muehlhoff
Russell
Choyke, Yates

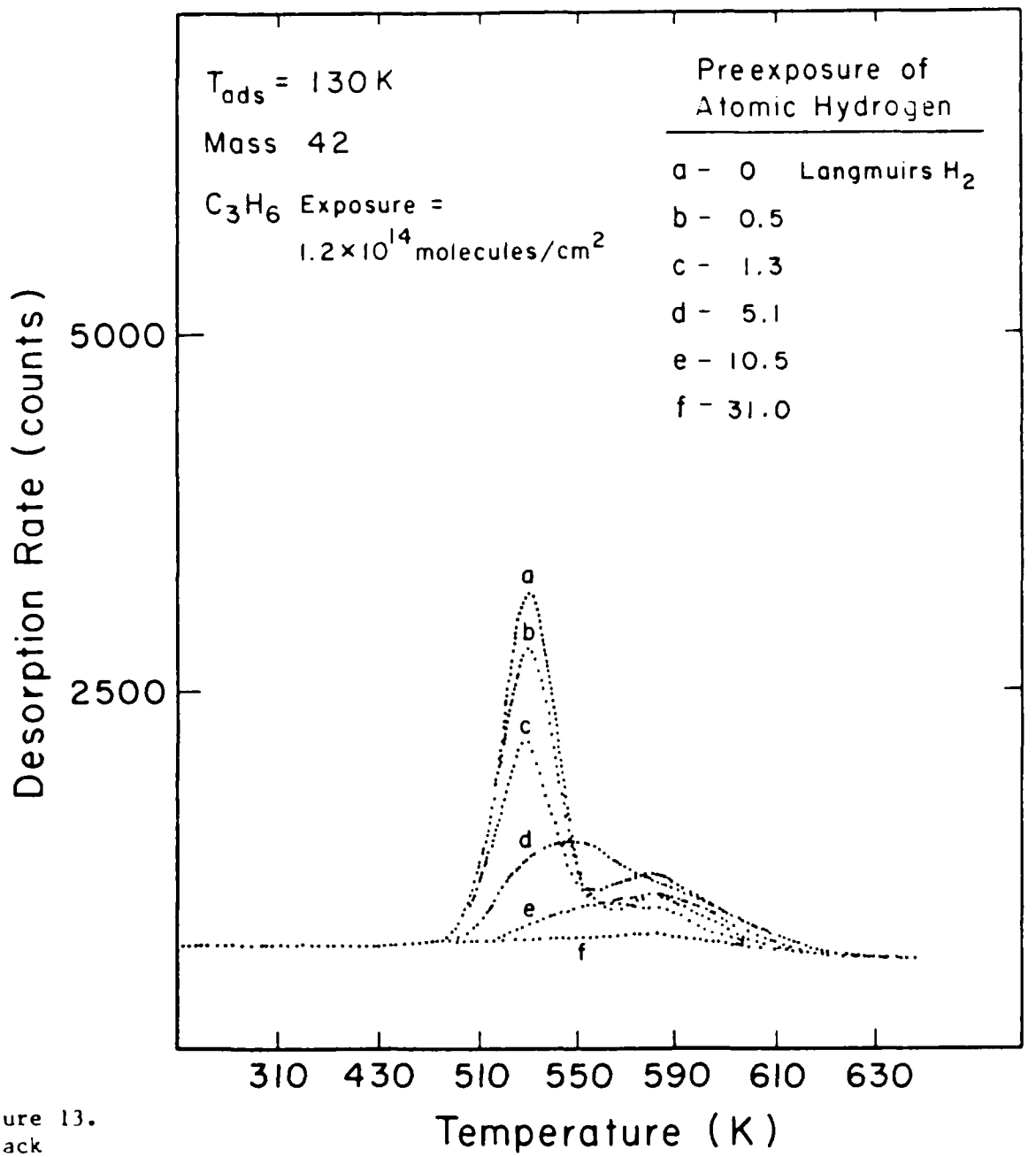

Figure 13.
Bozack
Muehlhoff
Russell
Choyke, Yates

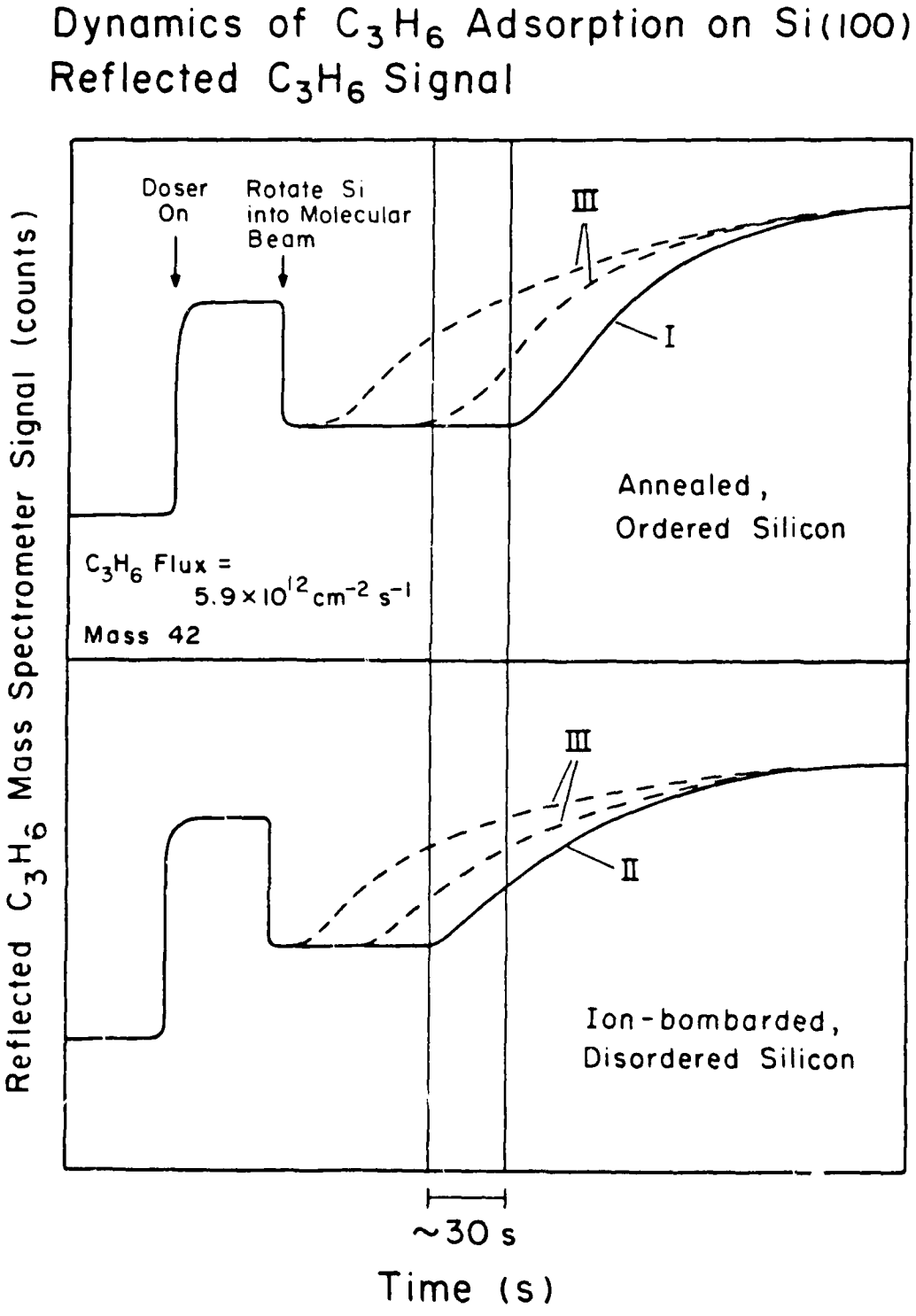

Figure 14.
Bozack
Muenlhoff
Russell
Choyke, Yates

REFERENCE 4

Surf. Sci. Letter
Date: 9 May 1986

Chemical Activity of the C=C Double Bond on Silicon Surfaces

M. J. Bozack, P. A. Taylor, W. J. Choyke,[a,b] and J. T. Yates, Jr.

Surface Science Center
Department of Chemistry
University of Pittsburgh
Pittsburgh, PA 15260

[a] Department of Physics, University of Pittsburgh, Pittsburgh, PA
[b] Westinghouse Research and Development Center, Pittsburgh, PA

Chemical Activity of the C=C Double Bond on Silicon Surfaces

M. J. Bozack, P. A. Taylor, W. J. Choyke,[a,b] and J. T. Yates, Jr.

Surface Science Center
Department of Chemistry
University of Pittsburgh
Pittsburgh, PA 15260

ABSTRACT

The adsorption kinetics of propylene, propane, and methane at 120 K on Si(100)-(2 x 1) are compared. Propane and methane have zero sticking probabilities at 120 K, while propylene reacts strongly with Si(100). The difference in sticking is shown in two ways. First, no kinetic uptake of propane and methane was observed during adsorption, while substantial uptake of propylene was observed. Second, measurements of the C(KLL)/Si(LVV) Auger peak-to-peak ratio before and after adsorption showed that no carbon was present on the surface after propane and methane exposures. It is shown therefore that the C=C double bond is an active molecular site for interaction with active sites on Si(100), whereas C-H and C-C single bonds are inactive at 120 K. This observation is of importance in models of chemical vapor deposition, plasma vapor deposition, and reactive ion etching.

[a] Department of Physics, University of Pittsburgh, Pittsburgh, PA
[b] Westinghouse Research and Development Center, Pittsburgh, PA

Despite the need to understand the chemistry of SiC formation on silicon surfaces, there have been few studies of the adsorption and decomposition of organic molecules on silicon. Klimesch et al. [1] have reported that the fraction of ethylene on Si(111) which desorbs without decomposition is about 20-30%. The ethylene was observed to desorb from two states at 600 K and 400 K with an activation energy of 0.48 eV and 0.22 eV respectively. Stroscio, Bare, and Ho [2] have studied methanol on Si(111) and also find decomposition of the molecule to produce a strongly-bound methoxy species (CH_3O) and SiH. In this Letter, we report studies which compare the adsorption of propylene, propane, and methane on Si(100).

Our goal in comparing propane and propylene adsorption was to determine the active site in the molecule causing reaction with the silicon surface. Propane is analogous to propylene except for the absence of the double bond. Previous studies showed that propylene adsorbs on Si(100) at 120 K with a sticking coefficient of ~ unity [3]. The present results extend this analysis and demonstrate that propane and methane do not adsorb on Si(100) at 120 K. The adsorption was carried out on both annealed (ordered) silicon and ion-prebombarded (disordered) silicon. Earlier, we showed that it is possible to enhance the reactivity of propylene with Si(100) by Si active site formation due to bombardment with Ar^+ ions [4]. The failure of propane and methane to adsorb on either annealed or ion-bombarded Si(100) shows that the C=C bond in propylene plays an important role in its surface chemistry on Si.

The experimental apparatus [4] used in this study consisted of a UHV chamber equipped with an Auger electron spectrometer, a quadrupole

mass spectrometer, a molecular beam doser, and a plasma discharge ion source. The base pressure of the system was 1×10^{-10} torr. The position of the crystal before and during gas dosing is shown in Figure 1.

The surface was cleaned in situ by sputtering with 2.0 keV Ar^+ ions followed by 5 minute thermal annealing at 1100 K. This procedure has been shown to produce a well-ordered Si(100)-(2 x 1) surface [5]. Temperatures were measured by an ice-junction referenced W-5% Re:W-26% Re thermocouple fastened inside a slot in the edge of the silicon crystal by an internal Ta spring contact. The sample was cooled to 120 K by means of circulating liquid nitrogen. The silicon base material was produced from Czochralski-grown B-doped material of 10 ohm-cm resistivity. The (100) face was oriented by Laue back reflection to ± 1 degree. Propylene (99.999%) was supplied commercially and purified using freeze-pump-thaw cycles. Propane (99.97%) and methane (99.99%) were of Matheson research purity and used without further purification. Subsequent checks with the mass spectrometer showed no evidence of contamination in the propylene and methane, while a small amount of argon was observed in the propane.

Kinetic observation of the reaction between the various gases and the Si(100) surface were examined by rotating the crystal surface into a molecular beam of the reactant molecules. The scattered molecular signal was monitored with the mass spectrometer. The results of such an experiment for the three gases are shown in Figure 2. The solid curves represent the interaction of the gas with a thermally annealed, ordered surface of Si(100), while the dashed curves represent the reaction with an ion-bombarded, disordered surface of Si(100). The molecular flux to the crystal was approximately the same in each case (6×10^{12} molecules/cm^2-sec), and the ion-bombarded surface was irradiated with

greater than 10^{15} Ar^+ ions/cm^2, corresponding to a heavily disordered surface. The mass peaks which were monitored were 42 (propylene), 44 (propane), and 16 (methane). After each exposure, an Auger spectrum of the surface was recorded to determine the amount of deposited carbon on the surface, as shown in the right hand portion of Figure 2.

Several observations may be made from the behavior of the scattered signals in Figure 2. With reference to propylene adsorption, during interception of the molecular beam by the crystal, the partial pressure of propylene rapidly decreases to a constant value as uptake by the crystal occurs. The constant value is indicative of an initial coverage-independent sticking coefficient, near unity. The sticking coefficient remains constant until a cutoff point is reached where the intensity of reflected C_3H_6 begins to rise as the reflection probability of the propylene increases. The existence of a constant sticking coefficient is indicative of adsorption kinetics where the propylene forms a mobile precursor on the surface before final attachment to the surface. The fact that the cutoff point is reached sooner on the ion-damaged Si(100) is indicative of the reduced adsorptive capacity of the crystal. This probably results from greater molecular fragmentation of propylene on the damaged surface with more than one active site being occupied by fragments of C_3H_6. That the initial behavior of the scattered signal is the same on the ion-bombarded and annealed surfaces is evidence for a sticking probability of unity for propylene on Si(100). It is unlikely that the sticking coefficient for an annealed and ion-bombarded surface would be identical unless the sticking probability was unity for both cases.

In contrast, the behavior of the scattered signal for reaction of C_3H_8 and CH_4 with Si(100) is radically different. When the crystal

is rotated into a molecular beam of these gases, no uptake of gas is observed. Rather, the scattered signal rises rapidly above the steady value set by the controlled leak in the absence of direct interception of the gas by the crystal. This is due to the incident molecular beam reflecting off the surface and directly into the ionizer of the quadrupole mass spectrometer. No difference was observed in the shape of the scattered signal (adsorption behavior) when the Si(100) surface was prebombarded with Ar^+ ions. Even with a damaged Si(100) surface, no adsorption of propane or methane is observed.

Corresponding to the kinetic measurements of gaseous uptake by Si(100) are Auger measurements taken after the gas exposure. In the case of propylene adsorption, exposure to ~ 10^{15} C_3H_6/cm^2 resulted in a saturated surface with an elemental composition of 75% Si and 25% C in the depth sampled by Auger spectroscopy [6]. Similar doses of C_3H_8 and CH_4 at 120 K resulted in zero detectable surface concentrations of carbon. With high doses of these molecules (e.g., > 10^{16} molecules/cm^2, well beyond comparable saturation doses of propylene), it was still not possible to detect any adsorbed carbon.

The observation of near-zero sticking coefficients for single-bonded hydrocarbon molecules on Si(100) has a number of implications for semiconductor-related process technologies. It is the existence of a double-bond that motivates reaction of hydrocarbon molecules with Si surfaces. At present, the form(s) of chemical bonding of propylene to Si(100) is not understood, and further studies using vibrational techniques are necessary.

The authors acknowledge support of this work from the Air Force Office of Scientific Research (AFOSR), under Contract No. F49260-84-C-0063DEF.

REFERENCES

[1] P. Klimesch, G. Meyer, and M. Henzler, Surf. Sci. 137, 79 (1984).

[2] J. A. Stroscio, S. R. Bare, and W. Ho, (submitted).

[3] M. J. Bozack, W. J. Choyke, L. Muehlnoff, and J. T. Yates, Jr., (submitted, J. Appl. Phys.).

[4] M. J. Bozack, W. J. Choyke, L. Muehlhoff, and J. T. Yates, Jr., (submitted, Surf. Sci.).

[5] J. C. Bean, G. E. Becker, P. M. Petroff, and T. E. Seidel, J. Appl. Phys. 48(3), 907 (1977).

[6] Estimates of the relative atomic concentration of C and Si in the Auger sampling depth were made using sensitivity factors found in: L. E. Davis, P. W. Palmberg, et al., Handbook of Auger Electron Spectroscopy, Physical Electronics Division, Perkin-Elmer Corp., Eden-Prairie, MN.

FIGURE CAPTIONS

Figure 1. Relative positions of the molecular beam doser, quadrupole mass spectrometer, and crystal during gas exposure.

Figure 2. The dynamics of hydrocarbon adsorption and Auger analysis of the surface after exposure to C_3H_6, C_3H_8, and CH_4. Propylene uptake is indicated by the drop in mass spectrometer intensity for mass 42 when the crystal is rotated into the C_3H_6 beam. Reflection, rather than uptake, is observed for C_3H_8 and CH_4 during interaction with Si(100). This is verified by Auger analysis of the surface after exposure. No adsorbed propane or methane are detected.

Apparatus for Measurement of Si(100) Adsorption Kinetics

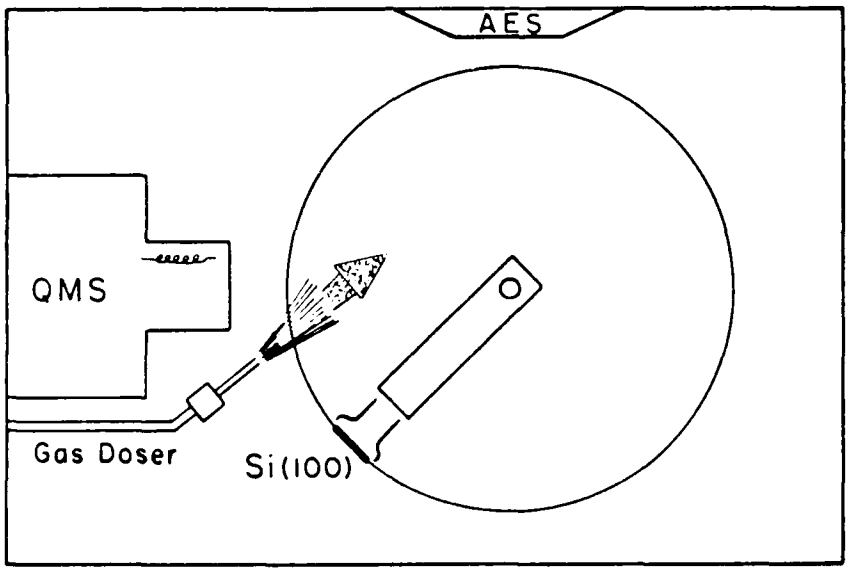

a) Crystal out of molecular beam.

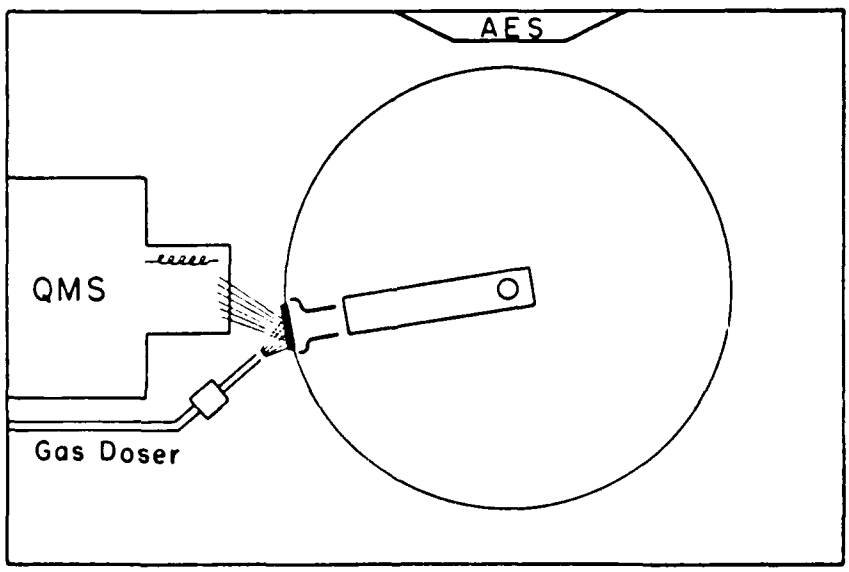

b) Molecular beam reflected into QMS by Si(100) crystal.

Figure 1.
Bozack
Taylor
Choyke
Yates

Hydrocarbon Adsorption on Si(100)

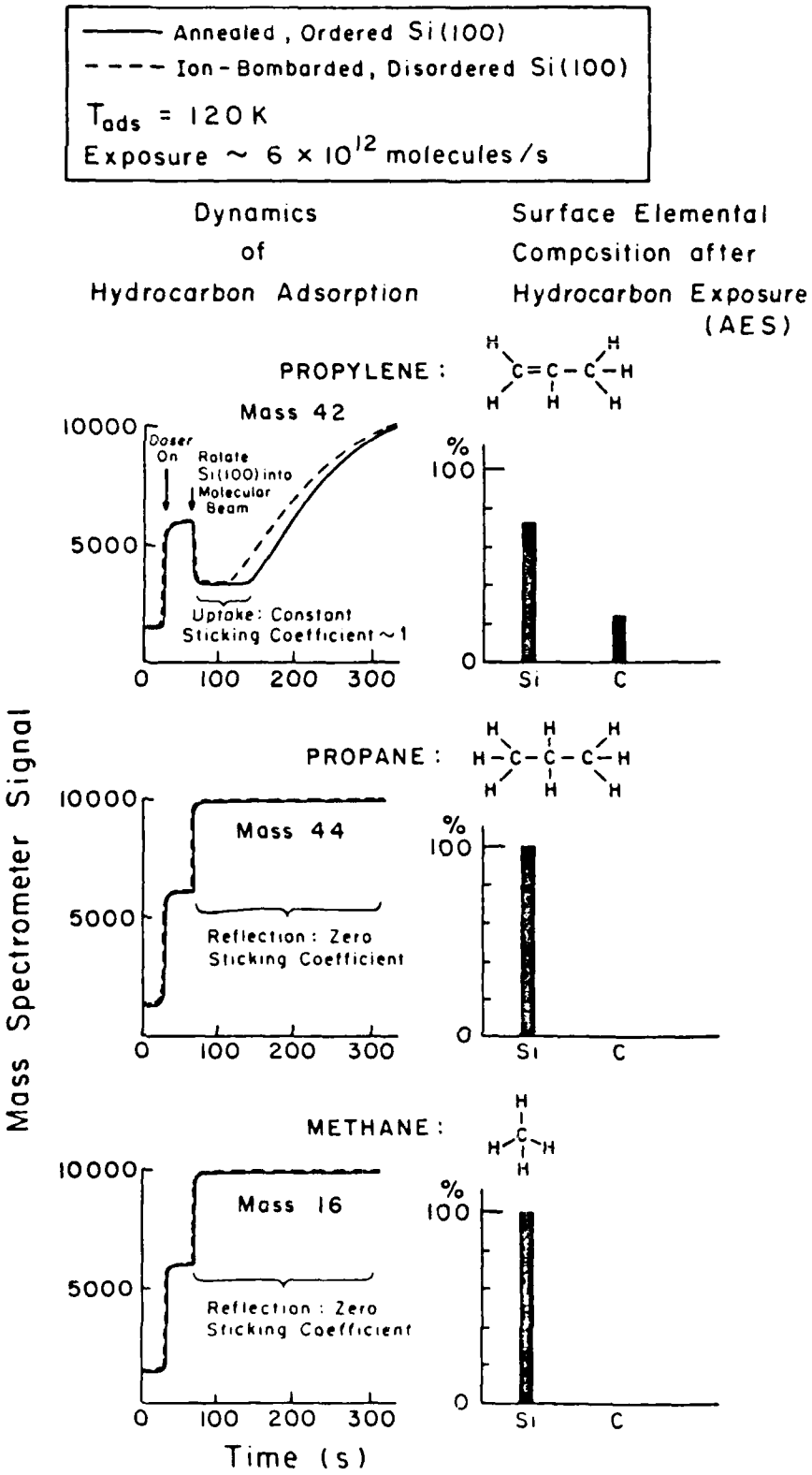

Figure 2.
Bozack
Taylor
Choyke
Yates

END

1-87

DTIC